



Contents lists available at ScienceDirect

European Journal of Medicinal Chemistry

journal homepage: <http://www.elsevier.com/locate/ejmech>

Research paper

Structure-guided optimization of 4,6-substituted-1,3,5-triazin-2(1H)-ones as catalytic inhibitors of human DNA topoisomerase II α Kaja Bergant^{a, c}, Matej Janežič^b, Katja Valjavec^a, Izidor Sosič^c, Stane Pajk^c, Martina Štampar^d, Bojana Žegura^d, Stanislav Gobec^c, Metka Filipič^d, Andrej Perdih^{a, *}^a National Institute of Chemistry, Hajdrihova 19, SI 1001, Ljubljana, Slovenia^b Laboratory for Structural Bioinformatics, RIKEN Center for Biosystems Dynamics Research, 1-7-22 Suehiro, Tsurumi, Yokohama, Kanagawa, 230-0045, Japan^c University of Ljubljana, Faculty of Pharmacy, Aškerčeva 7, SI 1000, Ljubljana, Slovenia^d National Institute of Biology, Department of Genetic Toxicology and Cancer Biology, Večna pot 111, 1000, Ljubljana, Slovenia

ARTICLE INFO

Article history:

Received 19 March 2019

Accepted 19 April 2019

Available online 25 April 2019

Keywords:

Human DNA topoisomerase II α

Catalytic inhibitors

Computer-aided drug design

In vitro studies

Anticancer agents

ABSTRACT

Human DNA topoisomerases represent one of the key targets of modern chemotherapy. An emerging group of catalytic inhibitors of human DNA topoisomerase II α comprises a new paradigm directed to circumvent the known limitations of topoisomerase II poisons such as cardiotoxicity and induction of secondary tumors. In our previous studies, 4,6-substituted-1,3,5-triazin-2(1H)-ones were discovered as catalytic inhibitors of topo II α . Here, we report the results of our efforts to optimize several properties of the initial chemical series that did not exhibit cytotoxicity on cancer cell lines. Using an optimized synthetic route, a focused chemical library was designed aimed at further functionalizing substituents at the position 4 of the 1,3,5-triazin-2(1H)-one scaffold to enable additional interactions with the topo II α ATP binding site. After virtual screening, selected 36 analogues were synthesized and experimentally evaluated for human topo II α inhibition. The optimized series displayed improved inhibition of topo II α over the initial series and the catalytic mode of inhibition was confirmed for the selected active compounds. The optimized series also showed cytotoxicity against HepG2 and MCF-7 cell lines and did not induce double-strand breaks, thus displaying a mechanism of action that differs from the topo II poisons on the cellular level. The new series represents a new step in the development of the 4,6-substituted-1,3,5-triazin-2(1H)-one class towards novel efficient anticancer therapies utilizing the catalytic topo II α inhibition paradigm.

© 2019 Elsevier Masson SAS. All rights reserved.

1. Introduction

Cancer is one of the most widespread diseases and a major cause of death worldwide. Recent predictions indicate that approximately 38.4% of men and women will be diagnosed with cancer at some point during their lifetimes [1]. The complex nature of cancer onset depends on genetic predispositions and environmental influences and combined with cancer tissue – drug pair specific response poses a great challenge for achieving successful treatment. In the seminal papers, Hanahan and Weinberg described several common traits, i.e., "Hallmarks of Cancer", that govern the transformation of normal cells to cancer cells during the multistep

development of human tumors. Research of novel molecules using an in-depth understanding of this underlying molecular mechanisms to provide efficient means to tackle cancer-related diseases is one of the priorities of the modern knowledge-based society [2–4].

A well-known treatment approach is to influence the cell replication mechanism. A large enzyme family of DNA topoisomerases catalyzes various topological changes of the DNA molecule, including catenation and decatenation, knotting and unknotting, and relaxation of the supercoiled plasmids [5], which link them to the processes of chromosome separation and segregation, transcription, and replication, and consequently to cancer where uncontrolled and increased cell division is one of its principal hallmarks [3,4]. Crystal structure of the complete topo II molecular motor from *Saccharomyces cerevisiae* (PDB: 4GFH), which has the same overall structure as its human counterpart, and the detailed topology of the ATP binding site of the human topo II α

* Corresponding author.

E-mail address: andrej.perdih@ki.si (A. Perdih).

(PDB: 1ZXM) are represented on Fig. 1A and comprise a good starting point for structure-based drug design.

Topoisomerases are broadly divided into two large groups - type I and type II topoisomerases. Type I topoisomerases act by generating transient single-strand breaks in the DNA molecule by forming a covalent phosphotyrosyl linkage [6]. In contrast, type II topoisomerases II belong to the GHKL (Gyrase, Hsp90, histidine kinase and MutL) family of enzymes [7–12]. They are also molecular motors that act via a complex catalytic cycle and catalyze topological changes of the DNA molecule by creating double-strand breaks in the first bound DNA molecule thus forming a covalent complex in order to allow the second DNA molecule to pass through the break [5]. For catalyzing DNA topological states, topo II utilizes the ATP chemical energy that is converted into directed molecular movement, fueling the action of this biological molecular motor [13–16]. Human topoisomerase II exists in α (170 kDa) and β (180 kDa) isoforms [5] that are products of two distinctive genes [17]. They share around 70% of sequence similarity but have different regulation during cell growth. Topo II α is greatly elevated in tumor cells, while the topo II β is present in proliferating and post mitotic cells. Human topo II α represents a main target of the type II family for cancer therapies [18–21].

Topoisomerase II inhibitors are traditionally divided into two large groups. The topo II poisons act by stabilizing the covalent topo II - DNA complex, which leads to permanent breaks in the cell DNA, resulting in chromosome translocations and apoptosis [22]. They are established molecules in clinical practice with anticancer drugs such as etoposide, doxorubicin, mitoxantron as its prime members [22–24]. Nonetheless, the utilization of this group of drugs is linked to severe effects, especially cardiotoxicity and induction of

secondary malignancies that are directly associated with the mechanism of action of topo II poisons – the prolonged stabilization of the transient covalent topo II - DNA complex [25,26]. This stimulated the development of a new diverse group of catalytic inhibitors of human topo II α that tries to take advantage of alternative inhibition paradigms [25,27,28]. Currently, four subgroups of catalytic inhibitors are described in the literature: compounds that prevent binding of the enzyme and DNA molecule, compounds that prevent the DNA cleavage, compounds that inhibit the ATP hydrolysis, and compounds that bind to the ATP binding site [22,29].

Our previous research activities have been involved in exploring the latter. So far, we have published several new classes of catalytic inhibitors, that target the ATP binding site possessing different core scaffolds mimicking the ATP adenine moiety functionality; among them triazin-2(1H)-ones [30], 1,3,5-triazines [31], 1H-pyrazolo [3,4] pyrimidines [32], 9H-purines [32] and 3-substituted-1H-indazoles [33].

One of our design starting points were the ATP-competitive catalytic topo II α inhibitors with the core 9H-purine scaffold, reported by the Novartis research group (Fig. 1B) [34]. By utilizing pharmacophore-based virtual screening, monocyclic 1,3,5-triazines compounds with this scaffold acting as a monocyclic replacement of the 9H-purine functionality that mimicked the ATP adenine moiety were discovered [31]. Subsequent optimization of the triazine scaffold resulted in the discovery of 4,6-substituted 1,3,5-triazinones-2(1H)-ones as fully characterized monocyclic catalytic inhibitors that however lacked cytotoxicity on cancer cells [30]. Still, this research provided valuable structure-activity relationship (SAR) data regarding the role of substituents introduced at the position 6 of the 1,3,5-triazin-2(1H)-one core [30].

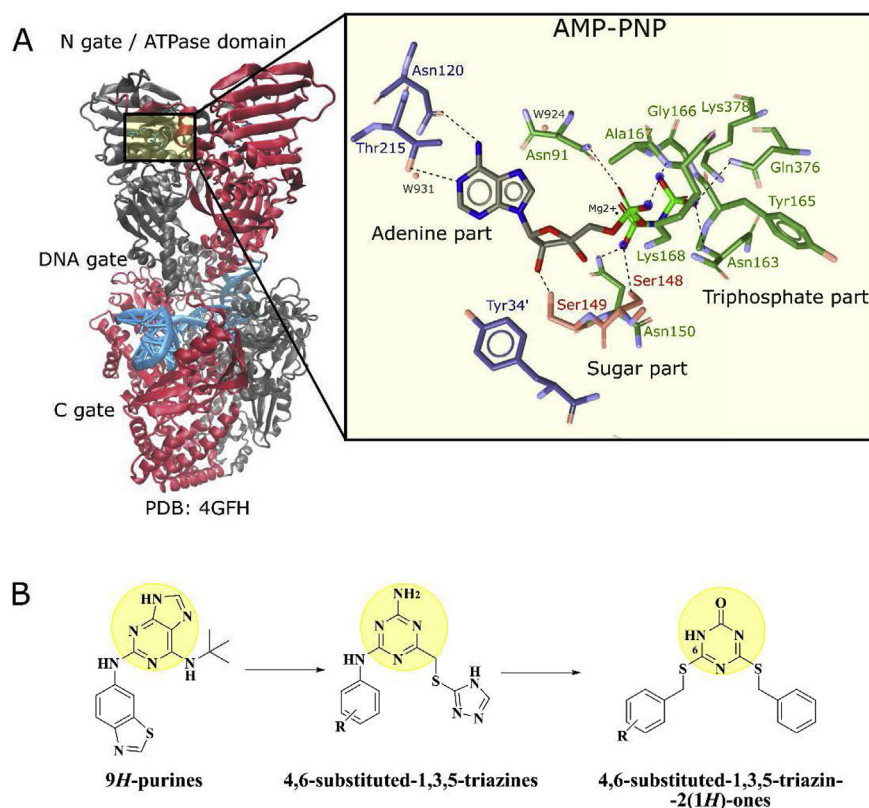


Fig. 1. (A) Crystal structure of the complete topo II molecular motor from *Saccharomyces cerevisiae* (PDB: 4GFH) and the detailed topology of the ATP binding site of the human topo II α (PDB: 1ZXM) that comprised the targeted site of our inhibitor design. (B) Outline of our previous design steps leading to the discovery of 1,3,5-triazin-2(1H)-ones as catalytic inhibitors.

This work is a continuation of our efforts to discover catalytic topo II α inhibitors that could lead to safer topo II α -based anticancer therapies. Here we report a structure-guided optimization of the 4,6-substituted-1,3,5-triazin-2(1H)-ones based on the generation and screening of a focused chemical library. The outline of our multistep procedure, which employed a combination of computational and experimental methods, is represented in Fig. 2.

Our main goal was to identify and introduce optimal substituents at the position 4 of the 1,3,5-triazin-2(1H)-one core to improve the inhibition potency and potentially obtain compounds that would display activity on the cellular level. We aimed to achieve this by exploiting additional interactions in the parts of the targeted ATP binding site where the ATP molecule's "ribose sugar" and "triphosphate" moieties interact. Based on the generated focused chemical library and structure-based virtual screening, selected derivatives were synthesized and experimentally evaluated for human topo II α inhibition. Inhibition of topoisomerase was first evaluated using the high-throughput screening (HTS) relaxation assay and for select active compounds the catalytic mechanism of topo II α inhibition was then investigated using decatenation, cleavage, competitive cleavage, and ATPase assays. Finally, cytotoxicity measurements were performed on HepG2 and MCF-7 cancer cell lines, followed by an analysis of the induction of the DNA double strand breaks (DSB) by the γ -H2AX assay on the HepG2 cell line to evaluate their genotoxic mechanism of activity even on the cellular level.

2. Results and discussion

2.1. Design of a focused library of 4,6-substituted-1,3,5-triazin-2(1H)-ones and a virtual screening

We recently reported monocyclic 4,6-substituted-1,3,5-triazin-2(1H)-one derivatives as novel catalytic inhibitors of human topo II α that bind to the ATPase domain where the ATP binding site is located [30]. During that study, we evaluated the influence of different substituents at the position 6 of the 1,3,5-triazin-2(1H)-one core while keeping the substitution position 4 fixed [30]. We noticed, that the most potent compounds included *m*-chloro (compound A) and *o*-fluoro (compound B) R¹ substituents at the 6-benzylthio moiety (Fig. 3A). By comparing our predicted binding

poses with that of the ATP extracted from PDB 1ZXN crystal structure we noticed that the nonsubstituted phenyl ring in this class of compounds overlapped with the position of the ribose sugar and triphosphate moieties of the ATP (Fig. 4, compound A). Our design was therefore focused on finding adequate R² substituents that would allow new compounds to form additional interactions in this part of the binding pocket that the previous series lacked. We particularly targeted new hydrogen bond interactions; residues Ser148, Ser149 and Asn150 in the "ribose sugar part" and residues Asn91, Ala167, Lys168, in the "triphosphate part" of the topo II α ATP binding site (Fig. S2).

We selected compounds A, B, and C as our starting point (Fig. 3A), kept the -triazin-2(1H)-one and its 6-halo R¹-substituted-phenyl ring fixed and set out to find which analogues could be reasonably synthesized. We utilized our reported synthetic route leading to 1,3,5-triazin-2(1H)-one compounds to construct a new library for virtual screening (Fig. 3B) [35]. In the first step, we identified 132 commercially available benzyl chloride analogs with diverse R² substitutions on the phenyl ring that could be introduced at the core scaffold position 4. Combining them with the selected compounds A–C resulted in the final focused virtual library comprised of 396 theoretical compounds. Before engaging in synthetic work we wanted to rationally evaluate which of these compounds were the most promising. Therefore, all 396 analogues were first docked into the ATP binding site of the human topo II α using GOLD docking package [36].

The docking poses were then visually analyzed with LigandScout software to check for interactions of these compounds with the topo II α ATP binding site [37]. Besides the already identified crucial hydrogen bond interaction with Asn120 and observed hydrophobic interactions between the phenyl ring and Ile125, Ile141 Thr159, Ala167 residues, we especially favoured those bound conformations that formed additional hydrogen bonds with the before mentioned targeted new residues; Ser148, Ser149 and Asn150 in the "ribose sugar part" and Asn91, Ala167, Lys168, residues in the "triphosphate part" of the ATP binding site. We also compared the binding modes with our reported model [30] for the active compound A–C. An example of a binding mode of the derivative 13 from the focused library (an optimized derivative of compound A) is displayed in the Fig. 4. The binding mode detected additional favourable interactions with Ala167/Lys168 residue pair in the

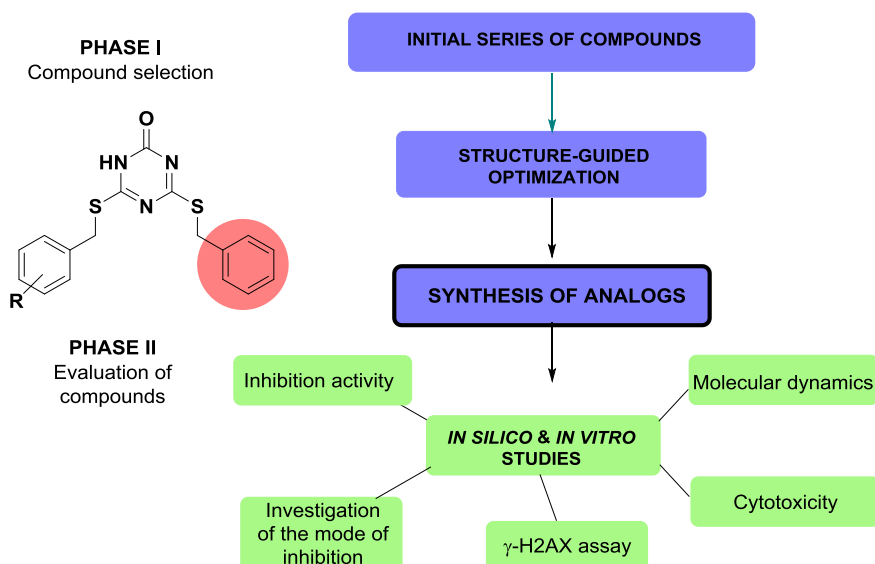


Fig. 2. Schematic representation of the computational and experimental workflow described in this work.

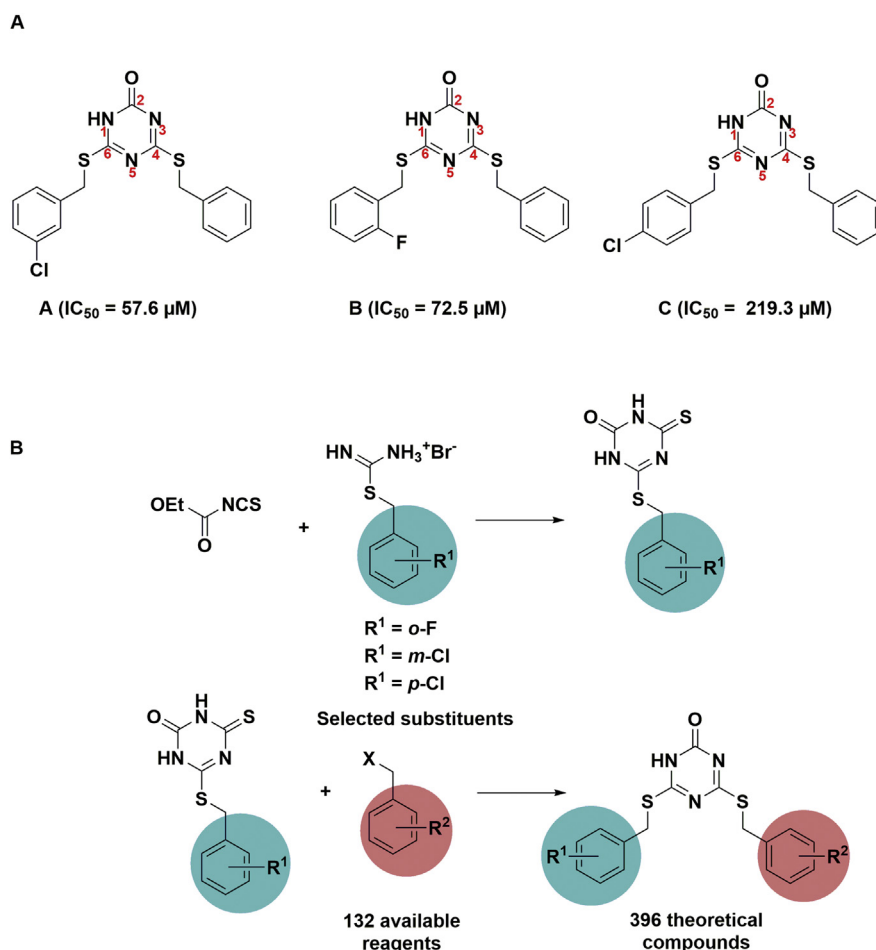


Fig. 3. (A) The reported 4,6-disubstituted 1,3,5-triazin-2(1H)-ones **A–C** define the position of the 6-based R^1 substituents in the optimized derivatives. (B) Synthetic route used in the design of a focused chemical library to additionally functionalize the position 4 of the 1,3,5-triazin-2(1H)-one by introducing different R^2 substituents.

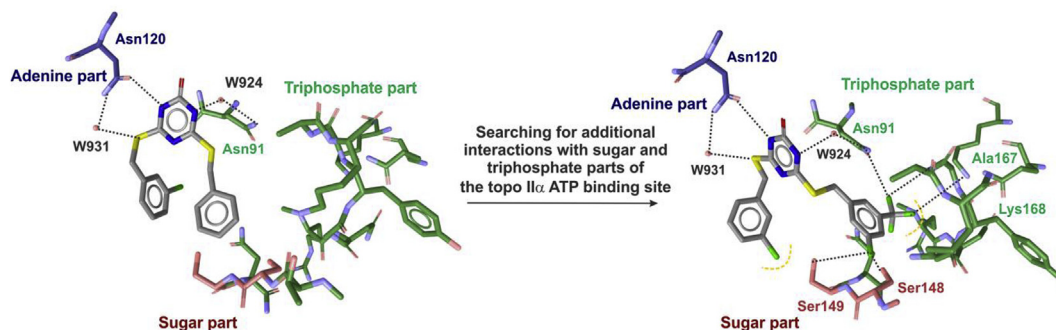


Fig. 4. Structure-based design of new 4,6-disubstituted-1,3,5-triazin-2(1H)-ones by virtual screening of a focused chemical library. (Left) Predicted binding mode of the initial compound **A** in the ATP binding site (PDB: 1ZXM) [30], (Right) Predicted binding mode of analogue **13**, which was selected for synthesis, with depicted additional interaction of the newly introduced substituents at the position 4.

“triphosphate” part as well as with the Ser148/Ser149 pair comprising the “ribose-sugar” part of the ATP binding site.

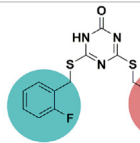
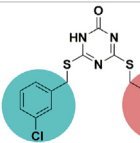
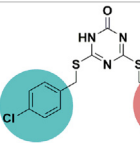
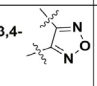
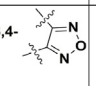
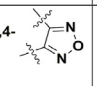
After visual analysis of molecular interactions of all docked compounds in the library, 12 synthons with new functionalities on the nonsubstituted phenyl core were selected. This resulted in 36 target compounds, **7–42**. Compounds selected for synthesis are shown in Table 1, where compound **B** derivatives containing the 4-(2-fluorobenzyl)thio moiety of the 1,3,5-triazin-2(1H)-one core are shown first, followed by both chlorine-containing derivatives of the

starting compounds **A** and **C**.

2.2. Synthesis of the optimized 4,6-disubstituted-1,3,5-triazin-2(1H)-ones

The selected 4,6-disubstituted 1,3,5-triazin-2(1H)-ones **7–42** were prepared as described previously [38]. Briefly, 6-substituted 4-thioxo-3,4-dihydro-1,3,5-triazine-2(1H)-ones **4–6** were prepared from the appropriate amidines **1–3** and ethoxycarbonyl

Table 1
Structures of the optimized 4,6-Substituted-1,3,5-triazin-2(1H)-ones selected for synthesis and their IC₅₀ values determined in the topo II α HTS screening relaxation assay.

								
Cpd.	R ²	IC ₅₀ [μM]	Cpd.	R ²	IC ₅₀ [μM]	Cpd.	R ²	IC ₅₀ [μM]
7	3,5-OMe	422.1	19	3,5-OMe	54.2	31	3,5-OMe	84.0
8	4-iPr	8.4	20	4-iPr	36.7	32	4-iPr	9.2
9		268.9	21		55.3	33		55.5
10	3-CONH ₂	716.0	22	3-CONH ₂	451.4	34	3-CONH ₂	293.4
11	2,6-F	170.8	23	2,6-F	165.6	35	2,6-F	43.2
12	3-COOH	>1000	24	3-COOH	388.1	36	3-COOH	>1000
13	3-CF ₃ , 5-F	8.1	25	3-CF ₃ , 5-F	34.4	37	3-CF ₃ , 5-F	8.4
14	2,4,5-F	164.1	26	2,4,5-F	36.6	38	2,4,5-F	38.6
15	4-CH(CH ₃)COOH	38.7	27	4-CH(CH ₃)COOH	145.1	39	4-CH(CH ₃)COOH	161.4
16	4-CH ₂ OH	156.6	28	4-CH ₂ OH	126.6	40	4-CH ₂ OH	154.9
17	3-OH	128.4	29	3-OH	45.3	41	3-OH	129.1
18	4-CF ₃	11.1	30	4-CF ₃	36.9	42	4-CF ₃	34.0

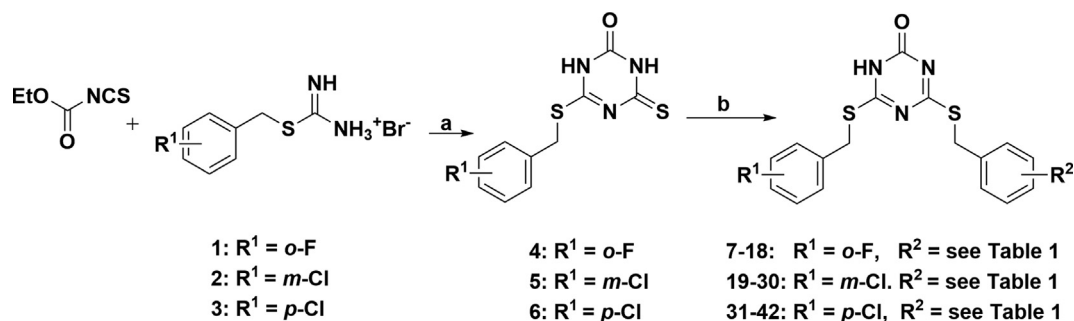
isothiocyanate, in the presence of 2 M NaOH in toluene at room temperature (Scheme 1). These products were then readily alkylated using various alkyl chlorides or bromides in a basic EtOH solution at room temperature to provide the 6-(2-fluorobenzylthio) (7–18), 6-(3-chlorobenzylthio) (19–30), and 6-(4-chlorobenzylthio) derivatives (31–42) in good yields. Further details along with compounds characterization data are available in the Experimental section.

2.3. In vitro human topo II α HTS inhibition assay and SAR of the optimized series

The 36 synthesized 4,6-disubstituted 1,3,5-triazin-2(1H)-ones 7–42 were then assayed for their human topo II α inhibitory activity utilizing a standard human topo HTS inhibition assay [39]. Etoposide, a clinically used anticancer drug, was used as a control compound and we experimentally determined the IC₅₀ value of 28.6 μM, comparable to the IC₅₀ of 60.3 μM reported in the literature [40]. Results of the HTS relaxation assay for the designed optimized compounds are available in Table 1 and it was gratifying to observe that several of them showed improvement in inhibition

of human topo II α over the initial compounds A–C of which compound A displayed the best IC₅₀ value, i.e. 57.6 μM [30]. The most active compound from the new series was compound 13 with an IC₅₀ of 8.1 μM, a considerable improvement over our original series, and superior potency compared to the reference drug compound etoposide. Moreover, these inhibition activities of the most potent compounds are fully comparable with the most potent topo II α compound classes reported to date in the literature [22,29,41].

The results of the inhibition assay provided further insights into the SAR data of this compound class. Overall, favorable contributions to the IC₅₀ values were associated with compounds possessing either fluoro substituents such as 3-CF₃, 5-F 4-CF₃ or the isopropyl substituent (4-CH(CH₃)₂) introduced on the previously unsubstituted phenyl ring. From the derivatives of compound B the most potent compounds were 8, 13, 15 and 18 with IC₅₀ values of 8.4 μM, 8.1 μM, 38.7 μM and 11.1 μM, respectively. All these compounds showed improvement in IC₅₀ value over the starting compound B, (IC₅₀ = 72.5 μM). Also, quite a few derivatives of the starting compounds A (IC₅₀ = 57.6 μM) and C (IC₅₀ = 219.3 μM) showed improvement in activities. Some examples of active compounds include 20, 25, 26, 30, 32, 37, 38 and 42 for which we



Scheme 1. General synthesis of compounds 4–6 and 7–42. Reagents and conditions: (a) 2 M NaOH, toluene, H₂O, rt, 24 or 48 h; (b) 2 M NaOH, EtOH, rt, 24 h.

determined IC_{50} values of 36.7 μ M, 34.4 μ M, 36.6 μ M, 36.9 μ M, 9.2 μ M, 8.4 μ M, 38.6 μ M and 34.0 μ M, respectively. Compounds with added strongly polar substituents, such as 3-COOH and 3-CONH₂ and 4-CH₂OH, did not show any improvement in IC_{50} values.

When analyzing the docking results, most additional interactions of the active compounds were associated with forming new interactions with Ser124, Ser149 and Asn150 residues in the “ribose sugar” part of the ATP binding site and with Ala167 and Lys168 residues located in its “triphosphate” part (see the docking modes for two additional compounds **18** and **25** in Supplementary material, Fig. S3).

2.4. Investigation of the topo II α inhibition mechanism

After obtaining initial results using HTS topo II α relaxation assay, we investigated the inhibitory mechanism of the optimized 4,6-substituted-1,3,5-triazin-2(1H)-ones in more detail. This is an important step of topo II α inhibitors evaluation since, due to the complex catalytic cycle [7], only additional specific assays can provide some key data points for elucidating their mode of action. For further assays, we selected compounds **13**, **18** with the 4-(2-fluorobenzyl)thio moiety, and compound **25** with the 4-(3-chlorobenzyl)thio substituent.

2.4.1. Human DNA II topoisomerase decatenation assay of human topo II α and topo II β isoforms

First, the decatenation assays for the selected three compounds **13**, **18** and **25** were performed to investigate whether they can inhibit the decatenation reaction. These experiments enable a direct visualization of the inhibition effect produced by the compounds. The kDNA decatenation assay was performed using kinetoplast (kDNA) as a substrate and etoposide - a known topo II α

anticancer agent - as a standard compound [42]. The results of the decatenation assay for selected compounds are presented in Fig. 5A. As shown here, all three compounds significantly inhibited the decatenation of kDNA in a concentration-dependent manner with the inhibitory activities greater than etoposide (see also Supplementary material, Table S2, for more details). Compound **25** was shown to be slightly more potent than compound **18**, but all compounds had their estimated IC_{50} values in the 3.9–31.5 μ M interval and full inhibition was observed already at 31.5 μ M. For comparison, etoposide fully inhibited decatenation at 125 μ M, while the inhibition was around 70% at 31.5 μ M. At the lowest investigated concentration of 3.9 μ M, etoposide and compound **13** did not inhibit the decatenation of kDNA; however, optimized 1,3,5-triazine-2(1H)-ones **18** and **25** still displayed 12% and 30% inhibition of decatenation, respectively.

We were further interested if the optimized inhibitors can act on both isoforms of the human topo II. Thus we performed the decatenation assays of human topo II β for the selected three compounds. Results showed that they fully inhibited human topo II β at concentrations 500 μ M, 125 μ M and 31.5 μ M. This was comparable to the inhibition observed for the topo II α isoform (Supplementary material, Table S2 and Table S3). Etoposide showed some selectivity for human topo II α versus human topo II β which is in accordance with the literature data [43,44] (for detailed comparison see Tables S2 and S3, Supplementary material).

It is important to point out that when designing catalytic topo II inhibitors, including those that target the ATP binding site, it has been established that inhibition of both isoforms could be desired [41]. In this respect, the catalytic inhibitors differ from the topo II poisons where selectivity for the topo II α isoform is favoured [41,45]. The topo II poisons turn the enzyme into a cellular toxin and, ideally, they should predominantly act on the fast growing tumor cells that have elevated concentrations of this enzyme. Due

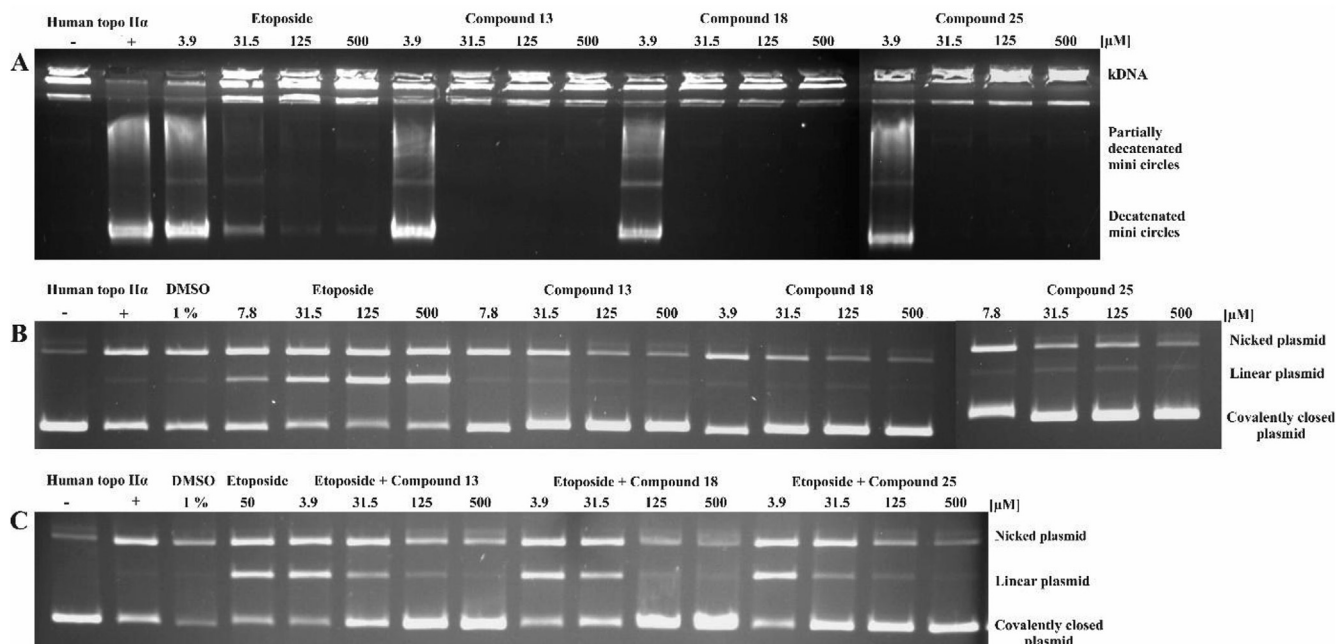


Fig. 5. Optimized 4,6-substituted-1,3,5-triazin-2(1H)-ones are catalytic inhibitors of human topoisomerase II α . (A) Topo II α decatenation assay results: compounds **13**, **18** and **25** inhibited DNA decatenation catalyzed by the human topo II α with inhibitory activities greater than the etoposide. Each reaction contained the same amount of human topo II α , the solvent DMSO (1%) and appropriate compound concentration, except the control reaction of kDNA which was performed in the presence of topo II α (+) and in the absence of topo II α (-) without any compounds. (B) Results of the topo II α cleavage assay for topo II poison etoposide and compounds **13**, **18** and **25**: unlike etoposide, compounds **13**, **18** and **25** do not function as human topo II α poison as they do not significantly increase the levels of linear DNA above that of the background level. (C) Results of the topo II α competitive cleavage assay: compounds antagonize the effect of etoposide at concentrations 31.5 μ M and above.

to very high similarity of sequences of both isoenzymes' ATP binding sites, inhibitor selectivity for this binding site would prove a challenging undertaking [41]. Experiments in mice have suggested that topo II α but not II β is essential for cell proliferation [46,47]; however, recent siRNA data showed that II β isoform can compensate II α depletion in certain cell lines [48]. Partial compensation should thus be taken into consideration when developing novel catalytic inhibitors and in this respect the inhibition of both topo II isoforms could be beneficial [41]. Additionally, it was reported that topoisomerase II β can be used as an anticancer target all by itself when targeting non-proliferative cells as well as cancer stem cells, and it was recently suggested as a potent target to counteract resistance of glioblastoma cells in glioblastoma therapy [49]. Further details of topo II α and topo II β decatenation assays are available in Supplementary material, Fig. S6 and Fig. S7.

2.4.2. Human DNA topoisomerase II α cleavage and competitive cleavage assays

The next important aspect of this investigation was to determine whether optimized compounds **13**, **18** and **25** acted as catalytic inhibitors, so topo II α cleavage assay was performed [42]. Human topo II α was incubated with the negatively supercoiled plasmid and four different concentrations of the investigated compounds **13**, **18** and **25** and topo II poison drug etoposide as a reference. The assay results presented in Fig. 5B clearly confirmed the expected poisonous activity of etoposide, which increased the amount of linear DNA with increasing concentrations of the drug. In contrast, the same titration with our compounds did not result in any significant amount of linear DNA above that of background level, confirming that the optimized compounds are indeed not topoisomerase poisons. Detailed results of the cleavage assay are available in Supplementary material, Table S4 and the gels of the parallel experiment (Fig. S8).

We also performed the competitive cleavage assay to investigate if compounds **13**, **18** and **25** could inhibit the formation of cleavage complexes induced by etoposide [42]. We performed the cleavage

assay at a constant concentration of the etoposide and four increasing concentrations of these 1,3,5-triazine-2(1H)-ones. The results are represented in Fig. 5C. We were pleased to observe that all three compounds successfully antagonized the effect of etoposide as a topoisomerase II poison in a concentration-dependent manner, with the antagonistic effect detected at concentrations 31.5 μ M and above. This suggests that compounds **13**, **18**, **25** act earlier in the human topo II α catalytic cycle than etoposide and indicates the ATP active site as the potential interacting site which is in accordance with our previous studies of this class [30]. The detailed results of competitive cleavage assays are available in Supplementary Material, Table S5 and results of second run in Fig. S9.

2.4.3. Competitive human topoisomerase II α ATPase assay

The results of the competitive cleavage topo II α assay confirmed that the optimized series acts earlier in the human topo II α catalytic cycle than the topo II poison etoposide, which is line with the ATP active site as the potential interacting site [30]. To investigate this further, we performed a competitive ATPase assay [42] to determine how substituted 1,3,5-triazine-2(1H)-one class can affect the ATP hydrolysis at different concentrations of the ATP. We chose compounds **18** and **25** as they performed best in the decatenation and cleavage assays. In Fig. 6, the observed rates of the ATP hydrolysis against the increased ATP concentration are plotted for different concentrations of both investigated inhibitors. The assay was carried out in two parallels for each compound. Additional data about this assay are further provided in Supplementary material, Table S6 and Table S7.

From the obtained graphs, it can be observed that the ATP hydrolysis was faster at lower concentrations of the inhibitors **18** and **25**, which shows that compounds have a substantial effect on the rate of the ATP hydrolysis. This is in line with the targeted mode of action of these compounds, acting via binding to the topo II α ATP binding site.

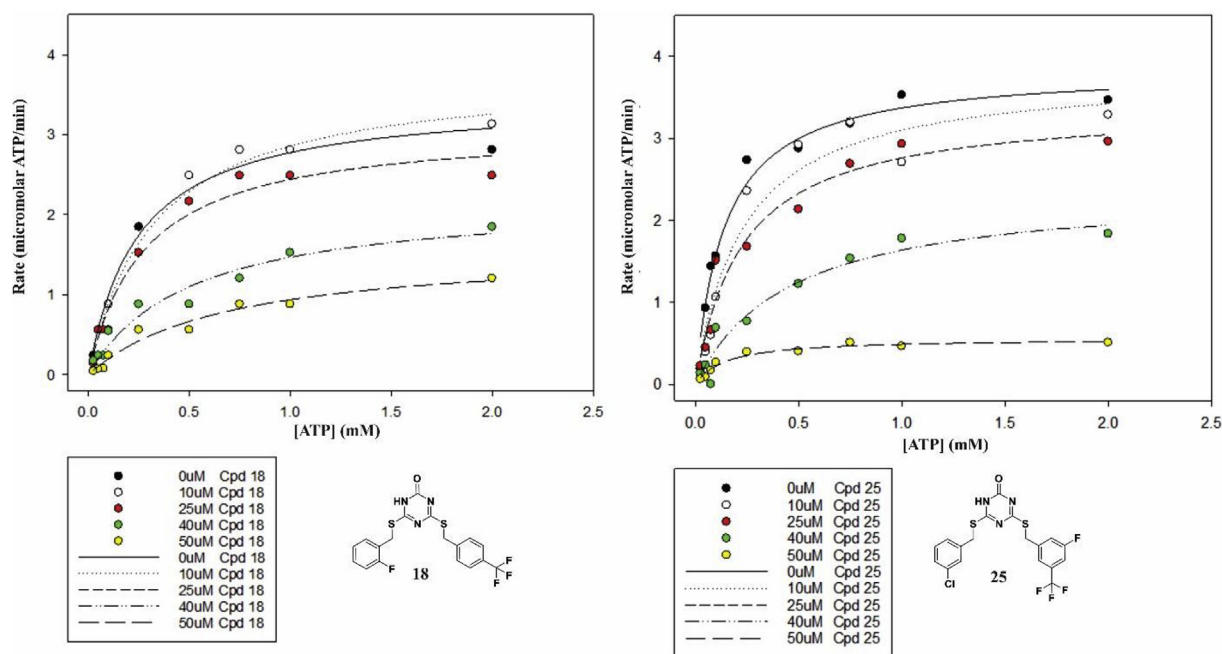


Fig. 6. Results of the competitive human topoisomerase II α ATPase assay. The rates of the ATP hydrolysis are plotted against the investigated ATP concentrations for compounds **18** (left) and compound **25** (right). Assay was performed in duplicates (Fig. S10).

2.5. Analysis of the target-ligand molecular interactions using molecular dynamics simulations and dynophore analysis

Our experimental data suggested that optimized series binds into the ATP binding site located on the human topo II α ATPase domain. Since molecular docking provides us only with a static binding pose of the target-ligand complex, we initiated molecular dynamics (MD) simulations using the proposed binding mode of the active compound **25** to gain information about its dynamical behavior [50]. We selected this compound since, as it will become apparent in the proceeding Section 2.6, it has a fully characterized inhibition mechanism and it performed best when evaluated on cancer cell lines. It is important to note that to the best of our knowledge no co-crystal structure of a small molecule inhibitor bound in the human topo II α ATP site has been reported so far. Using CHARMM we constructed a solvated target topo II α -ligand system that was then equilibrated and simulated in the 20 ns MD simulation as described in the Experimental section. Animations of the observed ligand-protein conformational space are available in the Supplementary material and a representative MD snapshot is presented in Fig. 7A.

First, we confirmed the overall stability of the proposed docked binding pose in the human topo II α binding site with the RMSD value of 2.59 ± 0.50 Å (Fig. S4). Next, we analyzed the ligand-target

interactions proposed by the GOLD docking model. The main hydrogen bond interaction between the amide oxygen of the Asn120 side chain and the triazin-2(*H*)-one scaffold nitrogen, was fully stable ($d = 2.9 \pm 0.2$ Å) during the simulation, serving as a main compound's anchor (Fig. 7B), which is in line with our previous model and simulations [30]. Since we mainly focused on optimizing the phenyl ring at the position 4 of 1,3,5-triazin-2(*H*)-one scaffold, we inspected new interactions between the F and CF₃ elements and the triphosphate and ribose sugar parts of the ATP binding site. We identified that interactions were present, yet higher average distance values were observed, for example with Thr147 4.1 ± 0.8 Å, with Gly164 4.6 ± 0.9 Å, with Ser148 5.0 ± 1.3 Å, and with Asn150 6.6 ± 1.4 Å (Fig. S4).

To rationalize this observation, we upgraded the geometrical MD analysis with a dynophore model a powerful new method of analysis of MD trajectories developed in the group of Prof. Wolber at the Freie Universität Berlin [51–53]. Dynophores aim at supplementing information provided by classical pharmacophores with statistical and sequential information as they include information gathered on all pharmacophores generated for each frame of the MD simulation [52,53]. In this way, the analysis of MD trajectories does not depend solely on the geometrical parameters such as intermolecular distances. This dynamical insight into the interaction pattern confirmed all predicted interactions (Fig. 7C). As

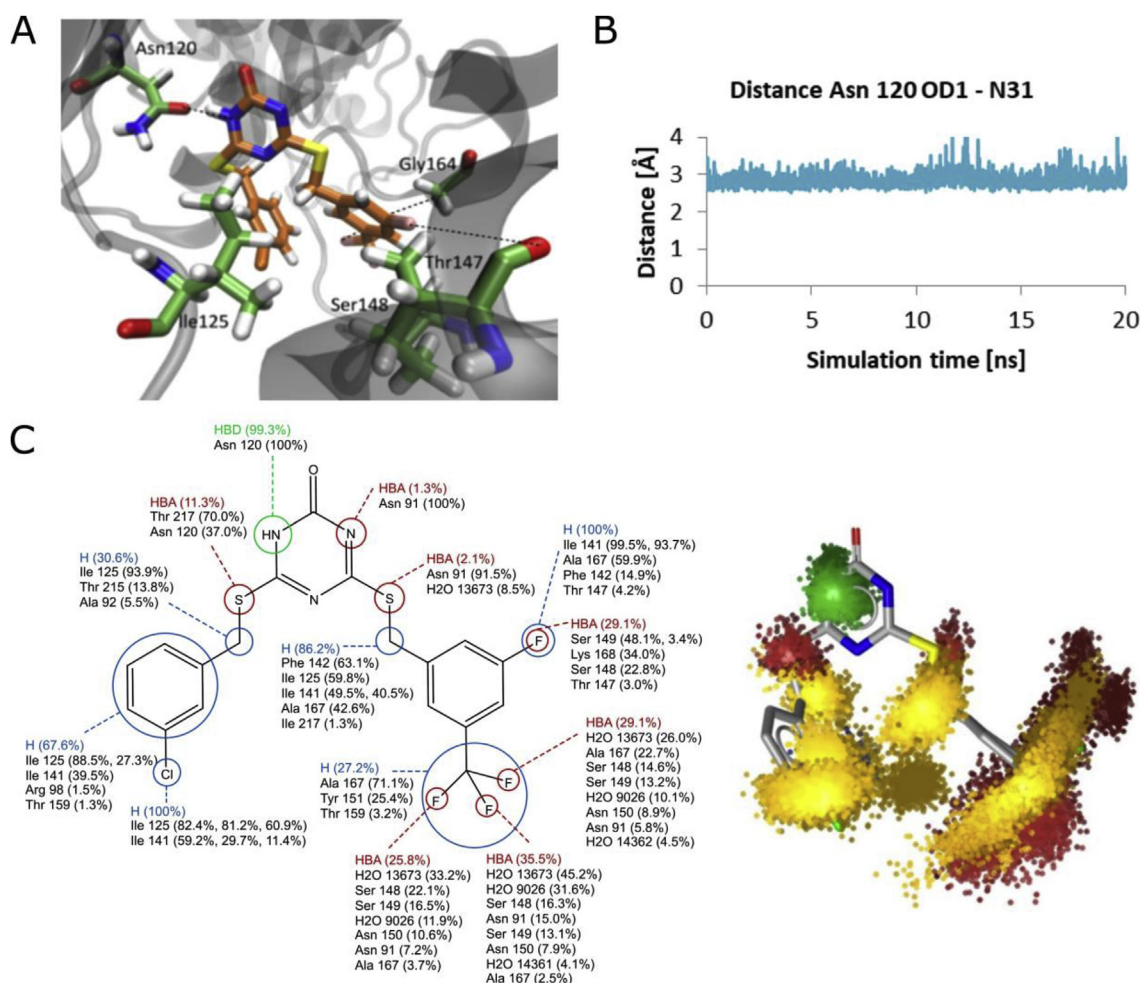


Fig. 7. (A) Representative MD snapshot of compound **25** in the ATP binding site of the human topo II α . (B) Time-dependence graph for the distance between the OD1 atom of Asn120 and the N31 nitrogen of compound **25**. (C) An overview of the interaction pattern obtained with dynophore analysis: (Left): Calculated percentage of the occurrence of a dynamic pharmacophore element on the basis of all frames broken into element-interacting amino acids pairs; (Right): Full calculated dynophore model of compound **25** presented with pharmacophore feature types – hydrogen bond donor, HBD (green), hydrogen bond acceptors, HBA (red) and hydrophobic area, H (yellow). (For interpretation of the references to colour in this figure legend, the reader is referred to the Web version of this article.)

expected, the hydrogen bond between the NH group of the 1,3,5-triazin-2(1H)-one fragment and oxygen of the Asn120 residue is present 99.3% of the simulation time. Also, hydrophobic interactions of the 6-(3-chlorobenzyl)thio moiety with Ile125 and Ile141 residues, as well as those between the hydrophobic elements present in the substituent at the position 4 of the 1,3,5-triazin-2(H)-one core and Ile125, Ile141 Thr159 and Ala167 residues, were detected and confirmed. Moreover, the dynophore presented a nice alternative interpretation of the positive impact resulting from the introduced fluoro-based substituents onto the second phenyl ring for topo II binding, as can be seen in Fig. 7C. Each F atom of the CF₃ group forms interactions one-third of the simulation time with the amino acid residues Thr147, Ser148, Asn150, Asn163 and Tyr165. Thus, the dynophore properly puts into perspective the slightly elevated average atom-pair distances we observed during the routine MD analysis; the CF₃ group is not fixed but rather it rotates and interacts with different amino acids in the binding site. Each of the four crucial pharmacophore elements describing compound's **25** molecular recognition is also presented separately in Fig. S5.

2.6. Cytotoxicity of the optimized compounds towards human cancer cell lines

Encouraged by the in vitro results of the optimized compounds on the enzymatic topo II α level we then determined the

cytotoxicity of all 36 synthesized compounds on the MCF-7 (human breast cancer) and HepG2 (human hepatoma) cancer cell lines using MTS assay. Both selected human cancer cell lines are representative and well-established systems for cell-based evaluation of potential anticancer compounds [42]. In the investigation of the original series of the 1,3,5-triazin-2(1H)-ones, no cytotoxicity on these cell lines was observed (data not shown).

The initial screening of the synthesized derivatives was performed by exposing exponentially growing cells to a 200 μ M concentration of the compounds for 24 h. The results revealed significant decrease of viability of MCF-7 and HepG2 cells for almost all compounds (Fig. 8). Only 8 and 7 compounds out of 36 tested did not significantly affect the viability of MCF-7 and HepG2 cells, respectively. Generally, HepG2 cells were more sensitive than MCF7 cells. Based on the screening results, we selected 12 compounds (**7**, **8**, **14**, **18**, **19**, **20**, **25**, **26**, **30**, **31**, **33**, **42**) that reduced HepG2 cell viability by more than 70% relative to the control and eight compounds (**7**, **14**, **19**, **20**, **25**, **26**, **31**, **33**) that reduced MCF-7 viability by more than 40% for the EC₅₀ determination.

These compounds were tested at graded concentrations to obtain dose-response curves. Etoposide was used as a positive control (PC) and at 200 μ M significantly decreased viability of HepG2 and MCF-7 cells. From the class of the investigated compounds, compounds **18** (EC₅₀ = 86.0 μ M) and **25** (EC₅₀ = 38.7 μ M) were the most active in the more sensitive cancer cell line HepG2.

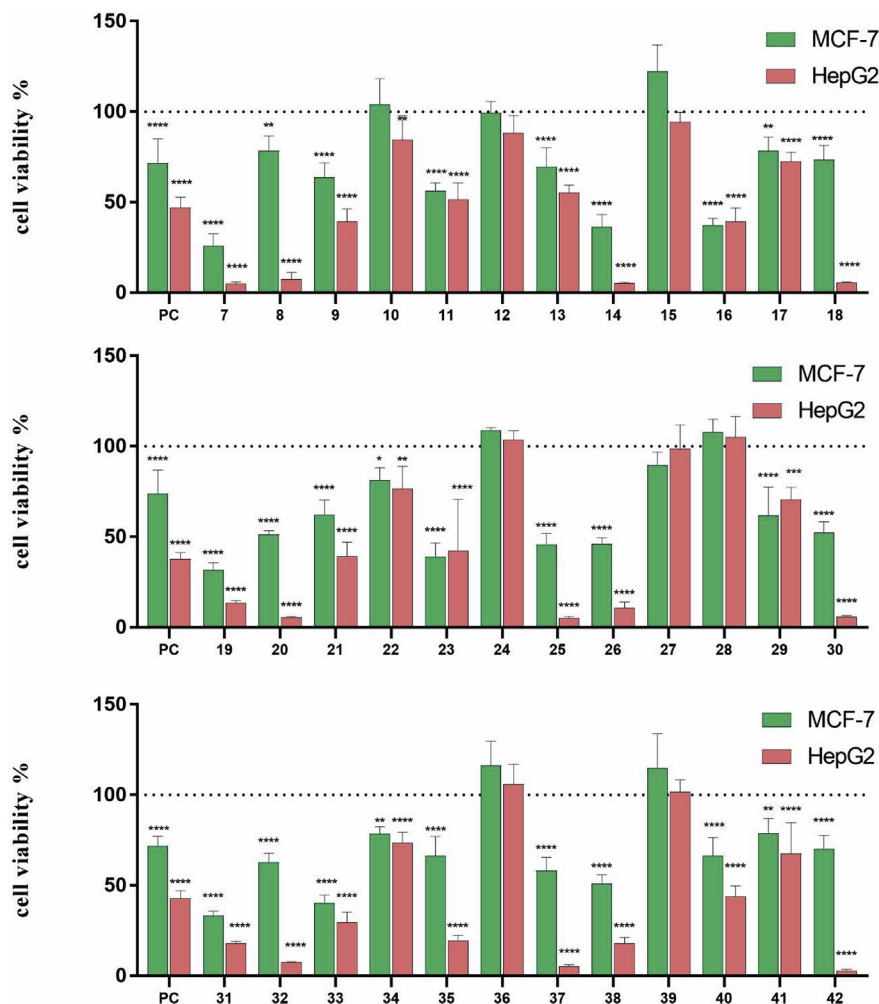


Fig. 8. Results of the MTS assay for all synthesized 4,6-substituted-1,3,5-triazin-2(1H)-ones **7–42**. HepG2 and MCF-7 cells were exposed to the investigated compounds at compounds concentration of 200 μ M for 24 h. As a positive control (PC), etoposide was used at 200 μ M and DMSO (0.5%) was used as solvent control.

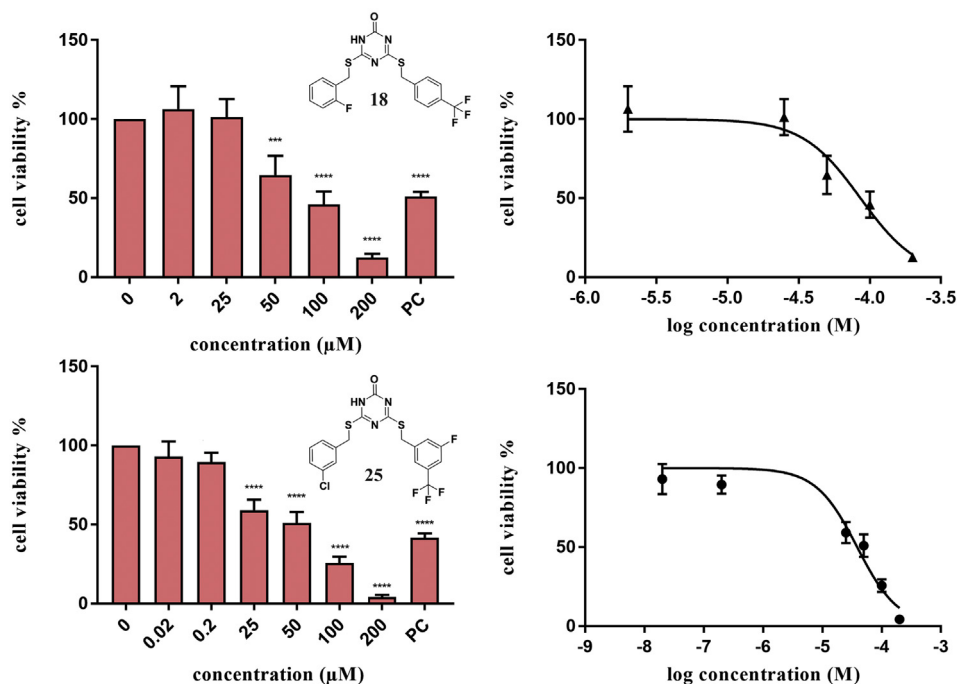


Fig. 9. Dose-response curves of inhibitors concentrations versus percent viability for the two most potent compounds **18** and **25** on the HepG2 cell line. Compound **25** was titrated at 0.02, 0.2, 25, 50, 100 and 200 μM , and compound **18** at 2, 25, 50, 100 and 200 μM . Experiments were performed in five parallels and SD values were calculated. Significant differences between the solvent control and treated cells were calculated using ANOVA (** $p < 0.01$, *** $p < 0.001$, **** $p < 0.0001$).

Significant decrease of the viability of the HepG2 cells was for compounds **18** and **25** observed at concentrations $\geq 50 \mu\text{M}$ and $25 \mu\text{M}$, respectively (Fig. 9). The obtained EC_{50} values are in the same range as the EC_{50} values obtained for etoposide, a well-known topoisomerase poison, with compound **25** being the most potent. The reported EC_{50} values for etoposide in HepG2 cells after 24 h treatment are $93.4 \mu\text{M}$ [54] or $60.5 \mu\text{M}$ [55]. The determined EC_{50} values for the remaining compounds are available in the Supplementary material, Table S8.

2.7. Analyses of the induction of the DNA double strand breaks by $\gamma\text{-H2AX}$ assay

Finally, the formation of the DNA double strand breaks (DSB) was analyzed by flow cytometry, measuring the fluorescent signals of individual cells indirectly through the detection of the $\gamma\text{-H2AX}$ foci. DSB are one form of DNA damage that can lead to chromosomal breakage and rearrangement [56]. DSB are also associated with the severe side effects of the topo II poisons, such as cardiotoxicity and induction of secondary malignancies [25,26,57]. The phosphorylated H2AX histones ($\gamma\text{-H2AX}$) can be used as biomarkers for the detection of DSB and DNA damage as they accumulate at sites, forming foci that correlate to DSB with a 1:1 ratio [58,59].

With the cleavage assay described in Section 2.4.2, we confirmed that the presented compounds act as catalytic inhibitors and not as topoisomerase poisons on the molecular level and with $\gamma\text{-H2AX}$ assay we sought to confirm the same, but on a cellular level. For the determination of the induction of DSB, HepG2 cells were selected as they showed higher sensitivity towards investigated compounds. The cells were exposed to the most active compound **25** (at 40 and $0.75 \mu\text{M}$) for 24 h. The results revealed no increase in the formation of DSBs after the exposure of HepG2 cells to compound **25**, while etoposide induced significant increase in DSB formation at $50 \mu\text{M}$ (Fig. 10). These results are in line with

different mechanisms of action of established topo II α poisons versus catalytic inhibitors at the cellular level. Nevertheless, these results represent only a first promising indication and a subsequent preclinical investigation is necessary to fully evaluate the activity of these compounds on the cellular level.

3. Conclusions

Cancer is, due to its widespread occurrence, a major health concern and its early detection and efficient treatment are important priorities of medical research activities. DNA topoisomerases, among them the human DNA topoisomerase II α , represent one of the core targets of current chemotherapy and a novel group of catalytic topo II α inhibitors is increasingly establishing itself as an attractive new inhibition paradigm that could circumvent the known limitations of topo II poisons such as cardiotoxicity and induction of secondary tumors.

In this study, we successfully undertook a structure-guided optimization of our previously discovered 4,6-substituted-1,3,5-triazin-2(1H)-ones using the principle of a focused chemical library generation followed by subsequent virtual screening. We introduced new substituents at the position 4 of the 1,3,5-triazin-2(1H)-one core trying to improve the inhibition potency. According to our binding model, this substituent orients itself towards the part of the II α ATP binding site where the ATP molecule's "ribose sugar" and "triphosphate" moieties interact and we sought to design analogs with functional groups that could exploit that. After virtual screening of the designed library using molecular docking 36 new derivatives (**7–42**) were synthesized and the best derivatives, i.e. compounds **13**, **18** and **25**, showed improved inhibition over the initial series as well superior inhibition compared to the established topo II poison etoposide. The inhibition activities of the most potent compounds are fully comparable with the most potent topo II α compound classes reported in the literature [22,23,29]. Further investigations confirmed that the optimized series acts via a

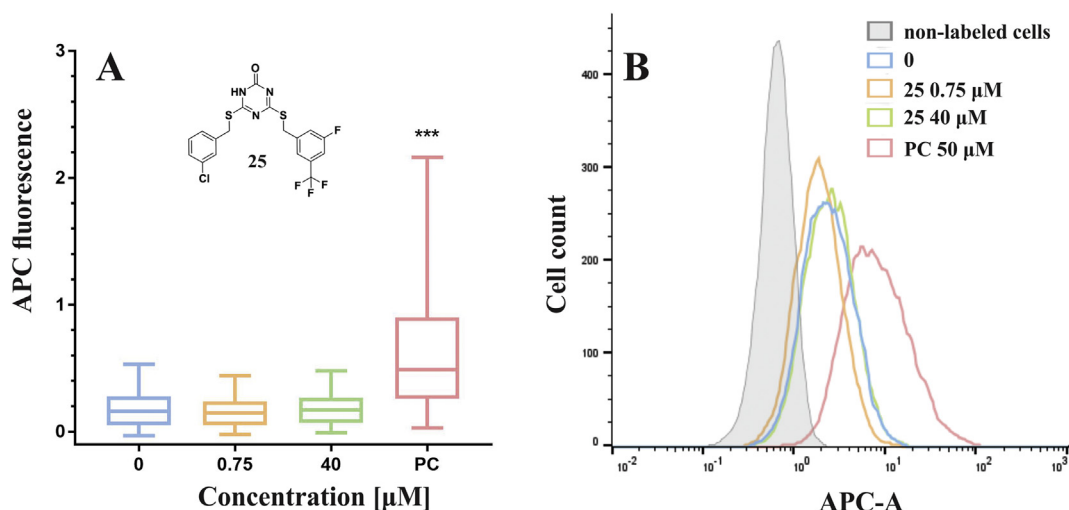


Fig. 10. Results of the analyses of the induction of the DNA double strand breaks by γ -H2AX assay. (A) Distribution of the fluorescent signals of individual cells in the samples is shown. Data are presented as quantile box plots. The edges of the box represent the 25th and 75th percentiles, the median is a solid line through the box, and the bars represent 95% confidence intervals. In each sample, 10^4 events were recorded, and experiments were repeated three times independently. Significant difference between treated cells and the solvent control (0) is indicated by * $p < 0.05$, ** $p < 0.01$ and *** $p < 0.001$. A solvent control (0.5% DMSO) and a positive control (50 μ M etoposide) were included in each parallel. (B) Representative histograms for non-labelled cells, vehicle control (0), compound **25** at 0.75 μ M and 40 μ M and etoposide at 50 μ M.

catalytic mechanism of topo II α inhibition as revealed by cleavage and competitive cleavage assays results. The compounds can influence the level of ATP hydrolysis in a concentration-dependent manner, which is in line with their targeted mode of action binding to the ATPase domain. Besides improvement in the inhibition potency, these compounds were the first of the 1,3,5-triazin-2(1H)-one chemical series to display cytotoxicity against MCF-7 and HepG2 cancer cell lines, being more active in the latter. Compounds also did not induce DSB in the HepG2 cell line. This substantiated the cytotoxic mechanism of action diverse from the topo II poisons even on the cellular level. The new optimized and characterized series of 4,6-substituted-1,3,5-triazin-2(1H)-ones comprises compounds with improved inhibition and cytotoxic properties that could pave the way to potentially safer future chemotherapies via topo II α molecular motor inhibition to treat various forms of cancer.

4. Experimental section

4.1. General chemistry methods

Reagents and solvents were obtained from commercial sources (Acros Organics, Aldrich, TCI Europe, Merck, Alfa Aesar, Fluorochem). Compounds 1–3 (2-(2-fluorobenzyl)isothiuronium bromide, 2-(3-chlorobenzyl)isothiuronium bromide, 2-(4-chlorobenzyl)isothiuronium bromide) were obtained from EvoBlocks. Solvents were distilled before use, while other chemicals were used as received. Reactions were monitored using analytical thin-layer chromatography plates (Merck 60 F254, 0.20 mm), and the components were visualized under UV light and/or through staining with the relevant reagent. Flash column chromatography was performed on Merck Silica Gel 60 (particle size 0.040–0.063 mm; Merck, Germany). ¹H and ¹³C NMR spectra were recorded on a Bruker Avance III 400 MHz spectrometer at 295 K. The chemical shifts (δ) are reported in parts per million (ppm) and are referenced to the deuterated solvent used. The coupling constants (J) are given in Hz, and the splitting patterns are designated as follows: s, singlet; br s, broad singlet; d, doublet; dd, double doublet; ddd, doublet of doublet of doublets; t, triplet; dq, doublet of quartets; qd, quartet of doublets; sept, septet; m, multiplet. Mass spectra data and high-resolution mass measurements were

performed on a VG-Analytical Autospec Q mass spectrometer at the Jožef Stefan Institute, Ljubljana, Slovenia. Analytical reversed-phase HPLC for the test compounds was performed on a Thermo Scientific DIONEX UltiMate 3000 system that was equipped with a photodiode array detector set to 254 nm. An XBridge C18 column (150 \times 4.6 mm; 3.5 μ m) was used, which was thermostated at 25 $^{\circ}$ C, with a flow rate of 1.0 mL/min and a sample injection volume of 10 μ L. An eluent system of A (H₂O/CH₃CN/HCOOH = 990/10/1) and B (CH₃CN/H₂O/HCOOH = 990/10/1) was used according to the general method of: 0–25 min, 80% A, 20% B \rightarrow 10% A, 90% B. The purities of the test compounds used for the biological evaluations were >95%, as determined by HPLC (unless noted otherwise).

4.2. Synthetic experimental procedures and compounds characterization data

4.2.1. General procedure for the synthesis of 6-substituted 4-thioxo-3,4-dihydro-1,3,5-triazine-2(1H)-ones **4–6**

To a solution of appropriate amidine 1–3 (1 equiv.) in H₂O (3 mL for 1.0 mmol of amidine), toluene (volume ranging from 5 mL for 1.0 mmol of amidine) was added and the mixture stirred vigorously. After 5 min, ethoxycarbonyl isothiocyanate (1.4 equiv.) in toluene (2 mL for 1.0 mmol of ethoxycarbonyl isothiocyanate) and NaOH (2 M, 1 mL for 1.0 mmol of amidine) were simultaneously added over a period of 5 min. Additional NaOH (2 M, 2 mL for 1.0 mmol of amidine) was added after 15 min and the reaction mixture was stirred for 48 h (for **4** and **5**) or 24 h (for **6**) at room temperature. The phases were then separated and the alkaline phases were acidified to pH 1 with H₂SO₄. The precipitate was formed, which was then filtered off and crystallized from CH₃CN.

6-((2-Fluorobenzyl)thio)-4-thioxo-3,4-dihydro-1,3,5-triazin-2(1H)-one (**4**). Yield, 82% (220 mg); white solid; R_f = 0.68 (CH₂Cl₂/MeOH = 9/1 + 1% AcOH); ¹H NMR (400 MHz, DMSO-*d*₆) δ 4.40 (s, 2H, SCH₂), 7.15–7.27 (m, 2H, Ar-H), 7.33–7.41 (m, 1H, Ar-H), 7.55 (td, J = 7.7, 1.7 Hz, 1H Ar-H), 12.49 (s, 1H, NH), 13.58 (br s, 1H, NH).

6-((3-Chlorobenzyl)thio)-4-thioxo-3,4-dihydro-1,3,5-triazin-2(1H)-one (**5**). Yield, 85% (857 mg); yellow solid; R_f = 0.08 (CH₂Cl₂/MeOH = 15/1); ¹H NMR (400 MHz, DMSO-*d*₆) δ 4.38 (s, 2H, SCH₂), 7.32–7.42 (m, 3H, Ar-H), 7.50–7.54 (m, 1H, Ar-H), 12.57 (s, 1H, NH), 13.70 (br s, 1H, NH); HRMS (ESI) m/z calculated for C₁₀H₉N₃OS₂Cl

$[M+H]^+$ 285.9876, found 285.9881.

6-((4-Chlorobenzyl)thio)-4-thioxo-3,4-dihydro-1,3,5-triazin-2(1H)-one (**6**). Yield, 82% (844 mg); white solid; R_f = 0.05 (CH₂Cl₂/MeOH = 15/1); ¹H NMR (400 MHz, DMSO-*d*₆) δ 4.37 (s, 2H, SCH₂), 7.36–7.42 (m, 2H, Ar-H), 7.42–7.48 (m, 2H, Ar-H), 12.57 (s, 1H, CONH), 13.68 (br s, 1H, CONH); HRMS (ESI) m/z calculated for C₁₀H₉N₃OS₂Cl $[M+H]^+$ 285.9876, found 285.9881.

4.2.2. General procedure for the synthesis of 4,6-disubstituted 1,3,5-triazin-2(1H)-ones 7–42

To a solution of compound **4**, **5**, or **6** (1 equiv.) in EtOH (3 mL for 1.0 mmol) and NaOH (2 M, 2 mL for 1.0 mmol), the corresponding benzyl halide (1.1 equiv.) was slowly added. The reaction mixture was stirred for 24 h at room temperature. After the reaction was complete, H₂O (4 mL for 1.0 mmol of starting compound) was added, followed by the addition of H₂SO₄ (2 M, until pH value reached 1). The precipitate formed was filtered off and the pure product obtained by crystallization from CH₃CN or trituration in *n*-hexanes and subsequent filtration, or column chromatography.

4-((3,5-Dimethoxybenzyl)thio)-6-((2-fluorobenzyl)thio)-1,3,5-triazin-2(1H)-one (**7**). The compound was purified by crystallization from CH₃CN. Yield, 53% (33 mg); white solid; R_f = 0.62 (CH₂Cl₂/MeOH = 9/1); ¹H NMR (400 MHz, DMSO-*d*₆) δ 3.70 (s, 6H, 2 × OCH₃), 4.29 (s, 2H, SCH₂), 4.39 (s, 2H, SCH₂), 6.39 (dd, J_1 = 2.3 Hz, J_2 = 2.3 Hz, 1H, Ar-H), 6.56–6.61 (m, 2H, Ar-H), 7.13–7.24 (m, 2H, Ar-H), 7.31–7.38 (m, 1H, Ar-H), 7.50 (td, J_1 = 7.7 Hz, J_2 = 1.7 Hz, 1H, Ar-H), 13.00 (br s, 1H, NHCO); ¹³C NMR (100 MHz, DMSO-*d*₆) δ 27.41, 33.76, 55.17, 99.33, 107.06, 115.44 (d, $^2J_{FC}$ = 21.0 Hz), 123.57 (d, $^2J_{FC}$ = 13.5 Hz), 124.59 (d, $^4J_{FC}$ = 3.5 Hz), 129.86 (d, $^3J_{FC}$ = 8.2 Hz), 131.42 (d, $^3J_{FC}$ = 3.6 Hz), 138.86, 160.45 (d, $^1J_{FC}$ = 246.0 Hz), 160.46, (signals for triazine were not observed); HRMS (ESI) m/z calculated for C₁₉H₁₉N₃O₃S₂F $[M+H]^+$ 420.0852, found 420.0841; HPLC purity, 98.77%, t_R = 16.41 min.

6-((2-Fluorobenzyl)thio)-4-((4-isopropylbenzyl)thio)-1,3,5-triazin-2(1H)-one (**8**). The compound was purified by crystallization from CH₃CN. Yield, 71% (39 mg); white solid; R_f = 0.61 (CH₂Cl₂/MeOH = 9/1); ¹H NMR (400 MHz, DMSO-*d*₆) δ 1.17 (d, J = 6.9 Hz, 6H, Ar-CH(CH₃)₂), 2.85 (sept, J = 6.9 Hz, 1H, Ar-CH(CH₃)₂), 4.34 (s, 2H, SCH₂), 4.40 (s, 2H, SCH₂), 7.14–7.24 (m, 4H, Ar-H), 7.28–7.39 (m, 3H, Ar-H), 7.50 (td, J_1 = 7.7 Hz, J_2 = 1.6 Hz, 1H, Ar-H), 13.05 (br s, 1H, NHCO); ¹³C NMR (100 MHz, DMSO-*d*₆) δ 23.84, 27.39, 33.13, 33.41, 115.43 (d, $^2J_{FC}$ = 21.1 Hz), 123.54 (d, $^2J_{FC}$ = 16.1 Hz), 124.57 (d, $^4J_{FC}$ = 3.5 Hz), 126.50, 129.03, 129.83 (d, $^3J_{FC}$ = 8.2 Hz), 131.41 (d, $^3J_{FC}$ = 3.6 Hz), 133.81, 147.69, 160.43 (d, $^1J_{FC}$ = 246.1 Hz), (signals for triazine were not observed); HRMS (ESI) m/z calculated for C₂₀H₂₁N₃O₃S₂F $[M+H]^+$ 402.1110, found 402.1114; HPLC purity, 92.36%, t_R = 20.72 min.

4-(Benzoc[1,2,5]oxadiazol-5-ylmethyl)thio)-6-((2-fluorobenzyl)thio)-1,3,5-triazin-2(1H)-one (**9**). The compound was purified by crystallization from CH₃CN. Yield, 45% (25 mg); white solid; R_f = 0.22 (CH₂Cl₂/MeOH = 20/1); ¹H NMR (400 MHz, DMSO-*d*₆) δ 4.39 (s, 2H, SCH₂), 4.51 (s, 2H, SCH₂), 7.11–7.23 (m, 2H, Ar-H), 7.29–7.38 (m, 1H, Ar-H), 7.49 (td, J_1 = 7.7 Hz, J_2 = 1.7 Hz, 1H, Ar-H), 7.64 (dd, J_1 = 9.3 Hz, J_2 = 1.4 Hz, 1H, Ar-H), 7.98–8.06 (m, 2H, Ar-H), 13.02 (br s, 1H, NHCO); ¹³C NMR (100 MHz, DMSO-*d*₆) δ 27.35, 33.48, 114.57, 115.43 (d, $^2J_{FC}$ = 21.1 Hz), 116.38, 123.38 (d, $^2J_{FC}$ = 14.4 Hz), 124.56 (d, $^4J_{FC}$ = 3.5 Hz), 129.89 (d, $^3J_{FC}$ = 8.2 Hz), 131.41 (d, $^3J_{FC}$ = 3.6 Hz), 134.61, 142.20, 148.28, 148.88, 160.41 (d, $^1J_{FC}$ = 246.1 Hz), (signals for triazine were not observed); HRMS (ESI) m/z calculated for C₂₂H₁₃N₅O₂S₂F $[M+H]^+$ 402.0495, found 402.0505; HPLC purity, 98.46%, t_R = 15.68 min.

3-(((6-((2-Fluorobenzyl)thio)-4-oxo-4,5-dihydro-1,3,5-triazin-2-yl)thio)methyl)benzamide (**10**). The compound was purified by crystallization from CH₃CN. Yield, 54% (38 mg); white solid; R_f = 0.46 (CH₂Cl₂/MeOH/CH₃COOH = 9/1/0.1); ¹H NMR (400 MHz,

DMSO-*d*₆) δ 4.32 (s, 2H, SCH₂), 4.34 (s, 2H, SCH₂), 7.10–7.22 (m, 2H, Ar-H), 7.26–7.44 (m, 3H, CONH₂ and Ar-H), 7.46–7.56 (m, 2H, Ar-H), 7.72–7.78 (m, 1H, Ar-H), 7.88–7.92 (m, 1H, Ar-H), 7.99 (br s, 1H, CONH₂), resonance for NHCO missing; ¹³C NMR (100 MHz, DMSO-*d*₆) δ 26.63, 32.92, 115.32 (d, $^2J_{FC}$ = 21.2 Hz), 124.49 (d, $^4J_{FC}$ = 3.5 Hz), 124.68 (d, $^2J_{FC}$ = 14.7 Hz), 126.12, 128.25, 128.34, 129.42 (d, $^3J_{FC}$ = 8.2 Hz), 131.35 (d, $^3J_{FC}$ = 3.8 Hz), 131.76, 134.47, 138.09, 149.97 (br s), 159.82 (br s), 160.41 (d, $^1J_{FC}$ = 245.6 Hz), 167.74, 176.00 (br s), (one of the signals for triazine was not observed); HRMS (ESI) m/z calculated for C₁₈H₁₆N₄O₂S₂F $[M+H]^+$ 403.0699, found 403.0702; HPLC purity, 92.87%, t_R = 10.35 min.

4-(((2,6-Difluorobenzyl)thio)-6-((2-fluorobenzyl)thio)-1,3,5-triazin-2(1H)-one (**11**). The compound was purified by crystallization from CH₃CN. Yield, 75% (34 mg); white solid; R_f = 0.54 (CH₂Cl₂/MeOH = 20/1); ¹H NMR (400 MHz, DMSO-*d*₆) δ 4.41 (s, 2H, SCH₂), 4.45 (s, 2H, SCH₂), 7.11–7.26 (m, 4H, Ar-H), 7.32–7.49 (m, 1H, Ar-H), 7.44 (tt, J_1 = 8.3 Hz, J_2 = 6.7 Hz, 1H, Ar-H), 7.52 (td, J_1 = 7.7 Hz, J_2 = 1.7 Hz, 1H, Ar-H), resonance for NHCO missing; ¹³C NMR (100 MHz, DMSO-*d*₆) δ 21.44, 27.34, 111.85 (d, $^2J_{FC}$ = 24.4 Hz), 111.91 (m, overlapping with signal at 111.85), 115.46 (d, $^2J_{FC}$ = 21.1 Hz), 123.49 (d, $^2J_{FC}$ = 14.8 Hz), 124.61 (d, $^4J_{FC}$ = 3.5 Hz), 129.90 (d, $^3J_{FC}$ = 8.2 Hz), 130.53 (t, $^3J_{FC}$ = 10.3 Hz), 131.48 (d, $^3J_{FC}$ = 3.6 Hz), 149.98, 160.46 (d, $^1J_{FC}$ = 246.1 Hz), 160.77 (dd, $^1J_{FC}$ = 248.7, 7.6 Hz), 169.03, 172.10 (br s); HRMS (ESI) m/z calculated for C₁₇H₁₃N₃O₃S₂F₃ $[M+H]^+$ 396.0452, found 396.0460; HPLC purity, 85.55%, t_R = 16.83 min.

3-(((6-((2-Fluorobenzyl)thio)-4-oxo-4,5-dihydro-1,3,5-triazin-2-yl)thio)methyl)benzoic acid (**12**). The compound was purified by crystallization from CH₃CN. Yield, 81% (46 mg); white solid; R_f = 0.73 (CH₂Cl₂/MeOH/CH₃COOH = 9/1/0.1); ¹H NMR (400 MHz, DMSO-*d*₆) δ 4.40 (s, 2H, SCH₂), 4.45 (s, 2H, SCH₂), 7.14–7.25 (m, 2H, Ar-H), 7.31–7.39 (m, 1H, Ar-H), 7.42–7.54 (m, 2H, Ar-H), 7.64 (m, 1H, Ar-H), 7.83–7.87 (m, 1H, Ar-H), 7.99–8.03 (m, 1H, Ar-H), 13.07 (br s, 2H, NHCO and COOH); ¹³C NMR (100 MHz, DMSO-*d*₆) δ 27.40, 33.17, 115.44 (d, $^2J_{FC}$ = 21.0 Hz), 123.49 (d, $^2J_{FC}$ = 14.7 Hz), 124.59 (d, $^4J_{FC}$ = 3.5 Hz), 128.33, 128.84, 129.85 (d, $^3J_{FC}$ = 8.0 Hz), 129.86, 131.04, 131.44 (d, $^3J_{FC}$ = 3.6 Hz), 133.51, 137.60, 153.32 (br s), 160.45 (d, $^1J_{FC}$ = 246.1 Hz), 167.08, 175.83 (br s); HRMS (ESI) m/z calculated for C₁₈H₁₅N₃O₃S₂F₃ $[M+H]^+$ 404.0539, found 404.0542; HPLC purity, 100.00%, t_R = 7.69 min.

4-(((3-Fluoro-5-(trifluoromethyl)benzyl)thio)-6-((2-fluorobenzyl)thio)-1,3,5-triazin-2(1H)-one (**13**). The compound was purified by crystallization from CH₃CN. Yield, 36% (28 mg); white solid; R_f = 0.24 (CH₂Cl₂/MeOH = 20/1); ¹H NMR (400 MHz, DMSO-*d*₆) δ 4.38 (s, 2H, SCH₂), 4.46 (s, 2H, SCH₂), 7.13–7.25 (m, 2H, Ar-H), 7.30–7.39 (m, 1H, Ar-H), 7.49 (td, J_1 = 7.7 Hz, J_2 = 1.7 Hz, 1H, Ar-H), 7.55–7.65 (m, 2H, Ar-H), 7.67–7.71 (m, 1H, Ar-H), 13.07 (br s, 1H, NHCO); ¹³C NMR (100 MHz, DMSO-*d*₆) δ 27.38, 32.56, 111.78 (dq, $^2J_{FC}$ = 24.5 Hz, $^3J_{FC}$ = 3.1 Hz), 115.42 (d, $^2J_{FC}$ = 21.1 Hz), 120.24 (d, $^2J_{FC}$ = 21.9 Hz), 121.89 (d, $^4J_{FC}$ = 3.1 Hz), 122.13 (m), 130.86 (dd, $^2J_{FC}$ = 32.6, $^3J_{FC}$ = 8.7 Hz), 123.41 (d, $^2J_{FC}$ = 15.4 Hz), 124.55 (d, $^4J_{FC}$ = 3.5 Hz), 129.88 (d, $^3J_{FC}$ = 8.3 Hz), 131.41 (d, $^3J_{FC}$ = 3.6 Hz), 142.18 (m), 160.44 (d, $^1J_{FC}$ = 246.1 Hz), 161.81 (d, $^1J_{FC}$ = 246.6 Hz) (signals for triazine were not observed); HRMS (ESI) m/z calculated for C₁₈H₁₃N₃O₃S₂F₅ $[M+H]^+$ 446.0420, found 446.0410; HPLC purity, 99.74%, t_R = 18.89 min.

6-((2-Fluorobenzyl)thio)-4-((2,4,5-trifluorobenzyl)thio)-1,3,5-triazin-2(1H)-one (**14**). The compound was purified by crystallization from CH₃CN. Yield, 46% (35 mg); white solid; R_f = 0.65 (CH₂Cl₂/MeOH = 20/1); ¹H NMR (400 MHz, DMSO-*d*₆) δ 4.35 (s, 2H, SCH₂), 4.39 (s, 2H, SCH₂), 7.13–7.27 (m, 2H, Ar-H), 7.31–7.40 (m, 1H, Ar-H), 7.45–7.68 (m, 3H, Ar-H), 13.11 (br s, 1H, NHCO); ¹³C NMR (100 MHz, DMSO-*d*₆) δ 26.68, 27.31, 106.07 (dd, $^2J_{FC}$ = 28.4 Hz, $^2J_{FC}$ = 21.4 Hz), 115.43 (d, $^2J_{FC}$ = 21.1 Hz), 119.16 (dd, $^2J_{FC}$ = 20.2 Hz, $^3J_{FC}$ = 4.8 Hz), 120.81 (m), 123.42 (d, $^2J_{FC}$ = 13.5 Hz), 124.57 (d, $^4J_{FC}$ = 3.5 Hz),

129.88 (d, $^3J_{\text{FC}} = 8.2$ Hz), 131.42 (d, $^3J_{\text{FC}} = 3.6$ Hz), 145.74 (ddd, $^1J_{\text{FC}} = 242.1$ Hz, $^2J_{\text{FC}} = 12.4$ Hz, $^4J_{\text{FC}} = 3.3$ Hz), 148.68 (td, $^1J_{\text{FC}} = 246.9$ Hz, $^2J_{\text{FC}} = ^3J_{\text{FC}} = 13.6$ Hz), 155.64 (ddd, $^1J_{\text{FC}} = 245.3$ Hz, $^3J_{\text{FC}} = 9.9$ Hz, $^4J_{\text{FC}} = 2.2$ Hz), 160.42 (d, $^1J_{\text{FC}} = 246.1$ Hz), (signals for triazine were not observed); HRMS (ESI) m/z calculated for $\text{C}_{17}\text{H}_{12}\text{N}_3\text{O}_5\text{S}_2\text{F}_4$ $[\text{M}+\text{H}]^+$ 414.0352, found 414.0371; HPLC purity, 93.73%, $t_{\text{R}} = 17.55$ min.

2-((4-(((6-((2-Fluorobenzyl)thio)-4-oxo-4,5-dihydro-1,3,5-triazin-2-yl)thio)methyl)phenyl)propanoic acid (**15**). The compound was purified by crystallization from CH_3CN . Yield, 37% (21 mg); white solid; $R_f = 0.26$ ($\text{CH}_2\text{Cl}_2/\text{MeOH} = 9/1$); ^1H NMR (400 MHz, $\text{DMSO}-d_6$) δ 1.33 (d, $J = 7.1$ Hz, 3H, Ar-(CH) CH_3), 3.65 (q, $J = 7.1$ Hz, 1H, Ar-(CH) CH_3), 4.35 (s, 2H, SCH_2), 4.39 (s, 2H, SCH_2), 7.13–7.27 (m, 4H, Ar-H), 7.32–7.40 (m, 3H, Ar-H), 7.50 (td, $J_1 = 7.1$ Hz, $J_2 = 1.6$ Hz, 1H, Ar-H), 12.70 (br s, 2H, NHCO and COOH); ^{13}C NMR (100 MHz, $\text{DMSO}-d_6$) δ 18.49, 27.39, 33.30, 44.34, 115.44 (d, $^2J_{\text{FC}} = 21.0$ Hz), 123.54 (d, $^2J_{\text{FC}} = 15.0$ Hz), 124.59 (d, $^4J_{\text{FC}} = 3.5$ Hz), 127.65, 129.18, 129.85 (d, $^3J_{\text{FC}} = 8.3$ Hz), 131.42 (d, $^3J_{\text{FC}} = 3.6$ Hz), 135.09, 140.51, 160.44 (d, $^1J_{\text{FC}} = 246.1$ Hz), 175.29 (br s); HRMS (ESI) m/z calculated for $\text{C}_{20}\text{H}_{19}\text{N}_3\text{O}_5\text{S}_2\text{F}$ $[\text{M}+\text{H}]^+$ 432.0852, found 432.0856; HPLC purity, 91.08%, $t_{\text{R}} = 13.42$ min.

6-((2-Fluorobenzyl)thio)-4-((4-(hydroxymethyl)benzyl)thio)-1,3,5-triazin-2(1H)-one (**16**). The compound was purified by crystallization from CH_3CN . Yield, 43% (25 mg); white solid; $R_f = 0.37$ ($\text{CH}_2\text{Cl}_2/\text{MeOH} = 9/1$); ^1H NMR (400 MHz, $\text{DMSO}-d_6$) δ 4.35 (s, 2H, SCH_2), 4.39 (s, 2H, SCH_2), 4.45–4.53 (m, 2H, Ar- CH_2OH), 5.12–5.25 (m, 1H, Ar- CH_2OH), 7.14–7.29 (m, 4H, Ar-H), 7.32–7.38 (m, 3H, Ar-H), 7.50 (td, $J_1 = 7.7$ Hz, $J_2 = 1.6$ Hz, 1H, Ar-H), 13.01 (br s, 1H, NHCO); ^{13}C NMR (100 MHz, $\text{DMSO}-d_6$) δ 27.37, 33.50, 62.60, 115.44 (d, $^2J_{\text{FC}} = 21.1$ Hz), 123.55 (d, $^2J_{\text{FC}} = 15.7$ Hz), 124.59 (d, $^4J_{\text{FC}} = 3.5$ Hz), 126.65, 128.83, 128.91 (d, signal is overlapping with signal at 128.83), 129.85 (d, $^3J_{\text{FC}} = 8.1$ Hz), 131.42 (d, $^3J_{\text{FC}} = 3.5$ Hz), 134.78, 141.87, 149.96, 160.43 (d, $^1J_{\text{FC}} = 246.0$ Hz), (one of the signals for triazine was not observed); HRMS (ESI) m/z calculated for $\text{C}_{18}\text{H}_{17}\text{N}_3\text{O}_5\text{S}_2\text{F}$ $[\text{M}+\text{H}]^+$ 390.0746, found 390.0742; HPLC purity, 81.18%, $t_{\text{R}} = 11.78$ min.

6-((2-Fluorobenzyl)thio)-4-((3-hydroxybenzyl)thio)-1,3,5-triazin-2(1H)-one (**17**). The compound was purified by crystallization from CH_3CN . Yield, 30% (29 mg); white solid; $R_f = 0.42$ ($\text{CH}_2\text{Cl}_2/\text{MeOH} = 9/1$); ^1H NMR (400 MHz, $\text{DMSO}-d_6$) δ 4.29 (s, 2H, SCH_2), 4.40 (s, 2H, SCH_2), 6.64–6.69 (m, 1H, Ar-H), 6.77–6.83 (m, 2H, Ar-H), 7.08–7.13 (m, 1H, Ar-H), 7.14–7.24 (m, 2H, Ar-H), 7.32–7.39 (m, 1H, Ar-H), 7.50 (td, $J_1 = 7.7$ Hz, $J_2 = 1.6$ Hz, 1H), 9.46 (s, 1H, Ar-OH), 13.05 (br s, 1H, NHCO); ^{13}C NMR (100 MHz, $\text{DMSO}-d_6$) δ 27.39, 33.63, 114.52, 115.43 (d, $^2J_{\text{FC}} = 21.1$ Hz), 115.75, 119.59, 123.54 (d, $^2J_{\text{FC}} = 9.5$ Hz), 124.59 (d, $^4J_{\text{FC}} = 3.5$ Hz), 129.58, 129.85 (d, $^3J_{\text{FC}} = 8.2$ Hz), 131.42 (d, $^3J_{\text{FC}} = 3.7$ Hz), 149.96, 157.48 (br s), 160.44 (d, $^1J_{\text{FC}} = 245.9$ Hz), (one of the signals for triazine was not observed); HRMS (ESI) m/z calculated for $\text{C}_{17}\text{H}_{13}\text{N}_3\text{O}_5\text{S}_2\text{F}$ $[\text{M}-\text{H}]^-$ 374.0439, found 374.0439; HPLC purity, 100.00%, $t_{\text{R}} = 13.03$ min.

6-((2-Fluorobenzyl)thio)-4-((4-(trifluoromethyl)benzyl)thio)-1,3,5-triazin-2(1H)-one (**18**). The compound was purified by crystallization from CH_3CN . Yield, 64% (49 mg); white solid; $R_f = 0.72$ ($\text{CH}_2\text{Cl}_2/\text{MeOH} = 9/1$); ^1H NMR (400 MHz, $\text{DMSO}-d_6$) δ 4.38 (s, 2H, SCH_2), 4.46 (s, 2H, SCH_2), 7.13–7.24 (m, 2H, Ar-H), 7.31–7.39 (m, 1H, Ar-H), 7.49 (td, $J_1 = 7.7$ Hz, $J_2 = 1.7$ Hz, 1H, Ar-H), 7.60–7.66 (m, 2H, Ar-H), 7.66–7.72 (m, 2H, Ar-H), 13.11 (br s, 1H, NHCO); ^{13}C NMR (100 MHz, $\text{DMSO}-d_6$) δ 27.37, 32.94, 115.43 (d, $^2J_{\text{FC}} = 21.1$ Hz), 120.17, 123.41 (d, $^2J_{\text{FC}} = 15.1$ Hz), 124.57 (d, $^4J_{\text{FC}} = 3.5$ Hz), 125.36 (q, $^2J_{\text{FC}} = 3.7$ Hz), 125.58, 127.91 (q, $^1J_{\text{FC}} = 31.9$ Hz), 128.29, 129.80, 129.92 (d, $^3J_{\text{FC}} = 3.8$ Hz), 131.42 (d, $^3J_{\text{FC}} = 3.6$ Hz), 142.10, 160.43 (d, $^1J_{\text{FC}} = 246.0$ Hz), (one of the signals for triazine was not observed); HRMS (ESI) m/z calculated for $\text{C}_{18}\text{H}_{12}\text{N}_3\text{O}_5\text{S}_2\text{F}_4$ $[\text{M}-\text{H}]^-$ 426.0363, found 426.0360; HPLC purity, 98.76%, $t_{\text{R}} = 18.67$ min.

6-((3-Chlorobenzyl)thio)-4-((3,5-dimethoxybenzyl)thio)-1,3,5-

triazin-2(1H)-one (**19**). The compound was purified by crystallization from CH_3CN (5 mL). Yield, 52% (49 mg); white crystals; $R_f = 0.37$ ($\text{CH}_2\text{Cl}_2/\text{MeOH} = 15/1$); ^1H NMR (400 MHz, $\text{DMSO}-d_6$) δ 3.71 (s, 6H, $2 \times \text{OCH}_3$), 4.28 (s, 2H, SCH_2), 4.36 (s, 2H, SCH_2), 6.39 (dd, $J_1 = 2.4$ Hz, $J_2 = 2.4$ Hz, 1H, Ar-H), 6.58 (d, $J = 2.4$ Hz, 2H, Ar-H), 7.31–7.39 (m, 3H, Ar-H), 7.48–7.50 (m, 1H, Ar-H), 13.03 (br s, 1H, NHCO); ^{13}C NMR (100 MHz, $\text{DMSO}-d_6$) δ 32.83, 33.72, 55.08, 99.21, 106.97, 127.26, 127.65, 128.80, 130.27, 132.88, 138.74, 139.61, 152.89 (br s), 160.36, 172.20 (br s), (one of the signals for triazine was not observed); HRMS (ESI) m/z calculated for $\text{C}_{19}\text{H}_{19}\text{N}_3\text{O}_3\text{S}_2\text{Cl}$ $[\text{M}+\text{H}]^+$ 436.0553, found 436.0553; HPLC purity, 98.78%, $t_{\text{R}} = 15.99$ min.

6-((3-Chlorobenzyl)thio)-4-((4-isopropylbenzyl)thio)-1,3,5-triazin-2(1H)-one (**20**). The compound was purified by trituration in *n*-hexanes and subsequent filtration. Yield, 70% (44 mg); white amorphous solid; $R_f = 0.32$ ($\text{CH}_2\text{Cl}_2/\text{MeOH} = 15/1$); ^1H NMR (400 MHz, $\text{DMSO}-d_6$) δ 1.17 (d, $J = 7.0$ Hz, 6H, Ar- $\text{CH}(\text{CH}_3)_2$), 2.80–2.91 (sept, $J = 7.0$ Hz, 1H, Ar- $\text{CH}(\text{CH}_3)_2$), 4.33 (s, 2H, SCH_2), 4.37 (s, 2H, SCH_2), 7.16–7.20 (m, 2H, Ar-H), 7.28–7.39 (m, 5H, Ar-H), 7.48–7.50 (m, 1H, Ar-H), 11.17 (br s, 1H, NHCO); ^{13}C NMR (100 MHz, $\text{DMSO}-d_6$) δ 23.77, 32.81, 33.05, 33.34, 126.41, 127.26, 127.66, 128.79, 128.95, 130.29, 132.88, 133.78, 139.64, 147.59, 149.87, 153.29 (br s), 176.52 (br s); HRMS (ESI) m/z calculated for $\text{C}_{20}\text{H}_{21}\text{N}_3\text{O}_3\text{S}_2\text{Cl}$ $[\text{M}+\text{H}]^+$ 418.0815, found 418.0808; HPLC purity, 97.85%, $t_{\text{R}} = 20.71$ min.

4-((Benzof[c][1,2,5]oxadiazol-5-ylmethyl)thio)-6-((3-chlorobenzyl)thio)-1,3,5-triazin-2(1H)-one (**21**). The compound was purified by crystallization from CH_3CN (10 mL). Yield, 58% (35 mg); white crystals; $R_f = 0.25$ ($\text{CH}_2\text{Cl}_2/\text{MeOH} = 15/1$); ^1H NMR (400 MHz, $\text{DMSO}-d_6$) δ 4.36 (s, 2H, SCH_2), 4.50 (s, 2H, SCH_2), 7.28–7.37 (m, 3H, Ar-H), 7.45–7.48 (m, 1H, Ar-H), 7.62 (dd, $J_1 = 9.3$ Hz, $J_2 = 1.5$ Hz, 1H, Ar-H), 7.98–8.00 (m, 1H, Ar-H), 8.02 (dd, $J_1 = 9.3$ Hz, $J_2 = 1.0$ Hz, 1H, Ar-H), resonance for NHCO missing; ^{13}C NMR (100 MHz, $\text{DMSO}-d_6$) δ 32.77, 33.39, 114.44, 116.25, 127.26, 127.60, 128.77, 130.23, 132.84, 134.46, 139.43, 142.11, 148.15, 148.75, 148.77, 153.27 (br s), 178.96 (br s); HRMS (ESI) m/z calculated for $\text{C}_{17}\text{H}_{13}\text{N}_5\text{O}_2\text{S}_2\text{Cl}$ $[\text{M}+\text{H}]^+$ 418.0199, found 418.0192; HPLC purity, 98.84%, $t_{\text{R}} = 15.42$ min.

3-(((6-((3-Chlorobenzyl)thio)-4-oxo-4,5-dihydro-1,3,5-triazin-2-yl)thio)methyl)benzamide (**22**). The compound was purified by crystallization from CH_3CN (25 mL). Yield, 31% (8 mg); white crystals; $R_f = 0.40$ ($\text{CH}_2\text{Cl}_2/\text{MeOH} = 5/1$); ^1H NMR (400 MHz, $\text{DMSO}-d_6$) δ 4.37 (s, 2H, SCH_2), 4.41 (s, 2H, SCH_2), 7.30–7.43 (m, 5H, Ar-H and CONH_2), 7.47–7.50 (m, 1H, Ar-H), 7.52–7.56 (m, 1H, Ar-H), 7.76 (dt, $J_1 = 7.7$ Hz, $J_2 = 1.4$ Hz, 1H, Ar-H), 7.90 (t, $J = 1.6$ Hz, 1H, Ar-H), 7.97 (br s, 1H, CONH_2), resonance for NHCO missing; ^{13}C NMR (100 MHz, $\text{DMSO}-d_6$) δ 32.86, 33.37, 126.35, 127.32, 127.70, 128.02, 128.22, 128.40, 128.84, 130.34, 132.91, 134.53, 137.48, 139.89, 149.90, 155.60 (br s), 167.56, 175.80 (br s); HRMS (ESI) m/z calculated for $\text{C}_{18}\text{H}_{16}\text{N}_4\text{O}_5\text{S}_2\text{Cl}$ $[\text{M}+\text{H}]^+$ 419.0403, found 419.0399; HPLC purity, 85.24%, $t_{\text{R}} = 10.36$ min.

6-((3-Chlorobenzyl)thio)-4-((2,6-difluorobenzyl)thio)-1,3,5-triazin-2(1H)-one (**23**). The compound was purified by trituration in *n*-hexanes and subsequent filtration. Yield, 67% (41 mg); white amorphous solid; $R_f = 0.31$ ($\text{CH}_2\text{Cl}_2/\text{MeOH} = 15/1$); ^1H NMR (400 MHz, $\text{DMSO}-d_6$) δ 4.38 (s, 2H, SCH_2), 4.43 (s, 2H, SCH_2), 7.09–7.18 (m, 2H, Ar-H), 7.31–7.48 (m, 4H, Ar-H), 7.49–7.51 (m, 1H, Ar-H), 13.10 (br s, 1H, NHCO); ^{13}C NMR (100 MHz, $\text{DMSO}-d_6$) δ 21.89, 33.31, 112.21 (d, $^2J_{\text{FC}} = 24.9$ Hz), 112.28 (dd, $^2J_{\text{FC}} = 19.0$ Hz, $^2J_{\text{FC}} = 12.5$ Hz), 127.81, 128.15, 129.30, 130.81, 130.94 (dd, $^3J_{\text{FC}} = 11.0$ Hz, $^3J_{\text{FC}} = 11.0$ Hz), 133.41, 140.01, 150.49, 153.70 (br s), 161.05 (dd, $^1J_{\text{FC}} = 248.7$ Hz, $^3J_{\text{FC}} = 8.1$ Hz), 175.94 (br s); HRMS (ESI) m/z calculated for $\text{C}_{17}\text{H}_{13}\text{N}_3\text{O}_2\text{F}_2\text{S}_2\text{Cl}$ $[\text{M}+\text{H}]^+$ 412.0157, found 412.0151; HPLC purity, 98.39%, $t_{\text{R}} = 16.71$ min.

3-(((6-((3-Chlorobenzyl)thio)-4-oxo-4,5-dihydro-1,3,5-triazin-2-yl)thio)methyl)benzoic acid (**24**). The compound was purified by crystallization from CH_3CN (5 mL). Yield, 52% (31 mg); white crystals; $R_f = 0.22$ ($\text{CH}_2\text{Cl}_2/\text{MeOH}/\text{CH}_3\text{COOH} = 9/1/0.1$); ^1H NMR

(400 MHz, DMSO- d_6) δ 4.37 (s, 2H, SCH₂), 4.43 (s, 2H, SCH₂), 7.30–7.38 (m, 3H, Ar-H), 7.45 (dd, $J_1 = 7.7$ Hz, $J_2 = 7.7$ Hz, 1H, Ar-H), 7.47–7.49 (m, 1H, Ar-H), 7.62–7.67 (m, 1H, Ar-H), 7.83 (dt, $J_1 = 7.8$ Hz, $J_2 = 1.3$ Hz, 1H, Ar-H), 7.98–8.00 (m, 1H, Ar-H), 13.03 (br s, 2H, COOH and NHCO); ¹³C NMR (100 MHz, DMSO- d_6) δ 32.90, 33.16, 127.34, 127.71, 128.30, 128.81, 128.86, 129.80, 130.35, 130.98, 132.93, 133.46, 137.51, 139.50, 149.92, 153.17 (br s), 167.03, 172.05 (br s); HRMS (ESI) m/z calculated for C₁₈H₁₅N₃O₃S₂Cl [M+H]⁺ 420.0243, found 420.0242; HPLC purity, 98.18%, $t_R = 12.16$ min.

6-((3-Chlorobenzyl)thio)-4-((3-fluoro-5-(trifluoromethyl)benzyl)thio)-1,3,5-triazin-2(1H)-one (**25**). The compound was purified by trituration in *n*-hexanes and subsequent filtration. Yield, 76% (61 mg); white amorphous solid; $R_f = 0.25$ (CH₂Cl₂/MeOH = 15/1); ¹H NMR (400 MHz, DMSO- d_6) δ 4.35 (s, 2H, SCH₂), 4.44 (s, 2H, SCH₂), 7.29–7.38 (m, 3H, Ar-H), 7.46–7.48 (m, 1H, Ar-H), 7.55–7.63 (m, 2H, Ar-H), 7.66–7.69 (m, 1H, Ar-H), resonance for NHCO missing; ¹³C NMR (100 MHz, DMSO- d_6) δ 32.46, 32.76, 111.70 (dq, ² $J_{FC} = 24.9$ Hz, ³ $J_{FC} = 3.7$ Hz), 120.15 (d, ² $J_{FC} = 22.0$ Hz), 122.00 (q, ³ $J_{FC} = 3.7$ Hz), 123.20 (qd, ¹ $J_{FC} = 272.2$ Hz, ⁴ $J_{FC} = 2.2$ Hz), 127.26, 127.62, 128.78, 130.78 (qd, ² $J_{FC} = 32.3$ Hz, ³ $J_{FC} = 8.8$ Hz), 130.32, 132.85, 139.48, 142.07 (d, ³ $J_{FC} = 5.9$ Hz), 148.81, 153.04 (br s), 161.75 (d, ¹ $J_{FC} = 247.2$ Hz), 172.74 (br s); HRMS (ESI) m/z calculated for C₁₈H₁₃N₃O₃S₂ClF₄ [M+H]⁺ 462.0125, found 462.0127; HPLC purity, 96.17%, $t_R = 18.82$ min.

6-((3-Chlorobenzyl)thio)-4-((2,4,5-trifluorobenzyl)thio)-1,3,5-triazin-2(1H)-one (**26**). The compound was purified by trituration in *n*-hexanes and subsequent filtration. Yield, 69% (44 mg); white amorphous solid; $R_f = 0.23$ (CH₂Cl₂/MeOH = 15/1); ¹H NMR (400 MHz, DMSO- d_6) δ 4.33 (s, 2H, SCH₂), 4.36 (s, 2H, SCH₂), 7.30–7.39 (m, 3H, Ar-H), 7.47–7.49 (m, 1H, Ar-H), 7.52–7.64 (m, 2H, Ar-H), resonance for NHCO missing; ¹³C NMR (100 MHz, DMSO- d_6) δ 26.76, 32.89, 106.06 (dd, ² $J_{FC} = 27.9$ Hz, ² $J_{FC} = 21.3$ Hz), 119.15 (dd, ² $J_{FC} = 19.8$ Hz, ³ $J_{FC} = 5.1$ Hz), 121.05 (dd, ² $J_{FC} = 18.4$ Hz, ³ $J_{FC} = 4.5$ Hz), 127.42, 127.60, 128.89, 130.41, 133.01, 139.60, 145.70 (ddd, ¹ $J_{FC} = 242.8$ Hz, ² $J_{FC} = 13.9$ Hz, ⁴ $J_{FC} = 4.4$ Hz), 148.64 (d, ¹ $J_{FC} = 248.7$ Hz, ² J_{FC} and ³ J_{FC} not observed), 150.01, 153.33 (br s), 155.65 (ddd, ¹ $J_{FC} = 245.0$ Hz, ³ $J_{FC} = 8.1$ Hz, ⁴ $J_{FC} = 2.9$ Hz), 175.42 (br s); HRMS (ESI) m/z calculated for C₁₇H₁₂N₃O₃S₂ClF₃ [M+H]⁺ 430.0062, found 430.0060; HPLC purity, 98.20%, $t_R = 17.42$ min.

2-(4-(((6-((3-Chlorobenzyl)thio)-4-oxo-4,5-dihydro-1,3,5-triazin-2-yl)thio)methyl)phenyl)propanoic acid (**27**). The compound was purified by column chromatography using CH₂Cl₂/MeOH/AcOH, 15/1/0.1 as an eluent. Yield, 56% (57 mg); white crystals; $R_f = 0.20$ (CH₂Cl₂/MeOH/CH₃COOH = 15/1/0.1); ¹H NMR (400 MHz, DMSO- d_6) δ 1.33 (d, $J = 7.2$ Hz, 3H, Ar-(CH)CH₃), 3.65 (q, $J = 7.2$ Hz, 3H, Ar-(CH)CH₃), 4.34 (s, 2H, SCH₂), 4.37 (s, 2H, SCH₂), 7.20–7.26 (m, 2H, Ar-H), 7.31–7.39 (m, 5H, Ar-H), 7.48–7.51 (m, 1H, Ar-H), 12.33 (br s, 2H, COOH and NHCO); ¹³C NMR (100 MHz, DMSO- d_6) δ 18.42, 32.86, 33.29, 44.29, 126.56, 126.88, 127.42, 127.59, 127.70, 128.84, 129.12, 130.33, 132.92, 140.43, 149.91, 153.13 (br s), 172.04 (br s), 175.25; HRMS (ESI) m/z calculated for C₂₀H₁₇N₃O₃S₂Cl [M-H][−] 446.0400, found 446.0403; HPLC purity, 95.52%, $t_R = 13.36$ min.

6-((3-Chlorobenzyl)thio)-4-((4-(hydroxymethyl)benzyl)thio)-1,3,5-triazin-2(1H)-one (**28**). The compound was purified by trituration in *n*-hexanes and subsequent filtration. Yield, 75% (53 mg); white amorphous solid; $R_f = 0.20$ (CH₂Cl₂/MeOH = 15/1); ¹H NMR (400 MHz, DMSO- d_6) δ 4.35 (s, 2H, SCH₂), 4.37 (s, 2H, SCH₂), 4.46 (s, 2H, Ar-CH₂OH), 7.21–7.28 (m, 2H, Ar-H), 7.31–7.39 (m, 5H, Ar-H), 7.48–7.50 (m, 1H, Ar-H), 11.17 (br s, 1H, CH₂OH), resonance for NHCO missing; ¹³C NMR (100 MHz, DMSO- d_6) δ 32.89, 33.50, 62.57, 126.50, 126.54, 126.62, 127.32, 127.70, 128.79, 128.85, 129.10, 130.35, 132.93, 149.92, 153.17 (br s), 172.96 (br s); HRMS (ESI) m/z calculated for C₁₈H₁₇N₃O₃S₂Cl [M+H]⁺ 406.0451, found 406.0441; HPLC purity, 88.83%, $t_R = 11.76$ min.

6-((3-Chlorobenzyl)thio)-4-((3-hydroxybenzyl)thio)-1,3,5-triazin-

2(1H)-one (**29**). The compound was purified by crystallization from CH₃CN (5 mL). Yield, 55% (24 mg); white crystals; $R_f = 0.30$ (CH₂Cl₂/MeOH = 15/1); ¹H NMR (400 MHz, DMSO- d_6) δ 4.28 (s, 2H, SCH₂), 4.37 (s, 2H, SCH₂), 6.66 (ddd, $J_1 = 8.0$ Hz, $J_2 = 2.4$ Hz, $J_3 = 0.9$ Hz, 1H, Ar-H), 6.77–6.81 (m, 2H, Ar-H), 7.02–7.13 (m, 1H, Ar-H), 7.31–7.39 (m, 3H, Ar-H), 7.48–7.50 (m, 1H, Ar-H), 9.47 (br s, 1H, Ar-OH), resonance for NHCO missing; ¹³C NMR (100 MHz, DMSO- d_6) δ 32.93, 33.65, 114.51, 115.74, 119.59, 127.36, 127.73, 128.87, 129.59, 130.38, 132.97, 137.70, 139.63, 149.95, 153.17 (br s), 157.44, 172.39 (br s); HRMS (ESI) m/z calculated for C₁₇H₁₅N₃O₃S₂Cl [M+H]⁺ 392.0294, found 392.0295; HPLC purity, 95.16%, $t_R = 13.04$ min.

6-((3-Chlorobenzyl)thio)-4-((4-(trifluoromethyl)benzyl)thio)-1,3,5-triazin-2(1H)-one (**30**). The compound was purified by trituration in *n*-hexanes and subsequent filtration. Yield, 75% (58 mg); white amorphous solid; $R_f = 0.39$ (CH₂Cl₂/MeOH = 15/1); ¹H NMR (400 MHz, DMSO- d_6) δ 4.36 (s, 2H, SCH₂), 4.44 (s, 2H, SCH₂), 7.30–7.38 (m, 3H, Ar-H), 7.46–7.49 (m, 1H, Ar-H), 7.59–7.64 (m, 2H, Ar-H), 7.65–7.70 (m, 2H, Ar-H), resonance for NHCO missing; ¹³C NMR (100 MHz, DMSO- d_6) δ 32.84, 32.91, 125.28 (q, ¹ $J_{FC} = 272.9$ Hz), 125.30 (q, ⁴ $J_{FC} = 4.4$ Hz), 127.31, 127.67, 127.82 (q, ² $J_{FC} = 31.5$ Hz), 128.83, 129.73, 130.16 (q, ³ $J_{FC} = 13.2$ Hz), 130.29, 132.93, 142.03, 149.91, 153.13 (br s), 171.91 (br s); HRMS (ESI) m/z calculated for C₁₈H₁₄N₃O₃S₂ClF₃ [M+H]⁺ 444.0219, found 444.0226; HPLC purity, 97.75%, $t_R = 18.62$ min.

6-((4-Chlorobenzyl)thio)-4-((3,5-dimethoxybenzyl)thio)-1,3,5-triazin-2(1H)-one (**31**). The compound was purified by crystallization from CH₃CN (5 mL). Yield, 52% (77 mg); white crystals; $R_f = 0.35$ (CH₂Cl₂/MeOH = 15/1); ¹H NMR (400 MHz, DMSO- d_6) δ 3.71 (s, 6H, 2 × OCH₃), 4.28 (s, 2H, SCH₂), 4.36 (s, 2H, SCH₂), 6.39 (dd, $J_1 = 2.4$ Hz, $J_2 = 2.4$ Hz, 1H, Ar-H), 6.57 (d, $J = 2.4$ Hz, 2H, Ar-H), 7.36–7.39 (m, 2H, Ar-H), 7.40–7.44 (m, 2H, Ar-H), resonance for NHCO missing; ¹³C NMR (100 MHz, DMSO- d_6) δ 32.78, 33.72, 55.12 (2C), 99.22, 107.00, 128.42, 130.82, 131.18, 131.95, 138.79, 149.90, 154.57 (br s), 160.40, 173.11 (br s); HRMS (ESI) m/z calculated for C₁₉H₁₉N₃O₃S₂Cl [M+H]⁺ 436.0556, found 436.0558; HPLC purity, 98.89%, $t_R = 16.53$ min.

6-((4-Chlorobenzyl)thio)-4-((4-isopropylbenzyl)thio)-1,3,5-triazin-2(1H)-one (**32**). The compound was purified by trituration in *n*-hexanes and subsequent filtration. Yield, 78% (50 mg); white amorphous solid; $R_f = 0.25$ (CH₂Cl₂/MeOH = 15/1); ¹H NMR (400 MHz, DMSO- d_6) δ 1.17 (d, $J = 6.9$ Hz, 6H, Ar-CH(CH₃)₂), 2.85 (sept, $J = 6.9$ Hz, 1H, Ar-CH(CH₃)₂), 4.33 (s, 2H, SCH₂), 4.36 (s, 2H, SCH₂), 7.16–7.21 (m, 2H, Ar-H), 7.27–7.31 (m, 2H, Ar-H), 7.35–7.39 (m, 2H, Ar-H), 7.40–7.44 (m, 2H, Ar-H), 13.02 (br s, 1H, NHCO); ¹³C NMR (100 MHz, DMSO- d_6) δ 23.81, 32.83, 33.11, 33.42, 126.46, 128.44, 128.99, 130.83, 131.99, 133.80, 136.09, 140.13, 147.65, 153.20 (br s), 173.84 (br s); HRMS (ESI) m/z calculated for C₂₀H₂₁N₃O₃S₂Cl [M+H]⁺ 418.0815, found 418.0821; HPLC purity, 97.87%, $t_R = 20.99$ min.

4-((Benzo[c] [1,2,5]oxadiazol-5-ylmethyl)thio)-6-((4-chlorobenzyl)thio)-1,3,5-triazin-2(1H)-one (**33**). The compound was purified by crystallization from CH₃CN (5 mL). Yield, 38% (13 mg); white crystals; $R_f = 0.32$ (CH₂Cl₂/MeOH = 15/1); ¹H NMR (400 MHz, DMSO- d_6) δ 4.35 (s, 2H, SCH₂), 4.49 (s, 2H, SCH₂), 7.32–7.36 (m, 2H, Ar-H), 7.37–7.42 (m, 2H, Ar-H), 7.61 (dd, $J_1 = 9.4$ Hz, $J_2 = 1.5$ Hz, 1H, Ar-H), 7.97–8.00 (m, 1H, Ar-H), 8.02 (dd, $J_1 = 9.3$ Hz, $J_2 = 1.0$ Hz, 1H, Ar-H), 13.13 (br s, 1H, NHCO); ¹³C NMR (100 MHz, DMSO- d_6) δ 32.79, 33.50, 114.51, 116.36, 128.45, 130.84, 131.21, 132.03, 134.57, 142.20, 148.27, 148.87, 149.97, 153.32 (br s), 175.40 (br s); HRMS (ESI) m/z calculated for C₁₇H₁₃N₅O₃S₂Cl [M+H]⁺ 418.0199, found 418.0192; HPLC purity, 96.18%, $t_R = 15.64$ min.

3-(((6-((4-Chlorobenzyl)thio)-4-oxo-4,5-dihydro-1,3,5-triazin-2-yl)thio)methyl)benzamide (**34**). The compound was purified by consecutive dissolving-filtration sequence in EtOH, acetone, MeOH, followed by trituration in *n*-hexanes. Yield, 36% (48 mg); white

amorphous solid; $R_f = 0.41$ ($\text{CH}_2\text{Cl}_2/\text{MeOH} = 9/1$); ^1H NMR (400 MHz, $\text{DMSO}-d_6$) δ 4.36 (s, 2H, SCH_2), 4.41 (s, 2H, SCH_2), 7.35–7.45 (m, 6H, Ar-H and CONH_2), 7.53 (dt, $J_1 = 7.8$ Hz, $J_2 = 1.4$ Hz, 1H, Ar-H), 7.76 (dt, $J_1 = 7.9$ Hz, $J_2 = 1.3$ Hz, 1H, Ar-H), 7.90 (t, $J = 1.5$ Hz, 1H, Ar-H), 7.97 (br s, 1H, CONH_2), 13.03 (br s, 1H, NHCO); ^{13}C NMR (100 MHz, $\text{DMSO}-d_6$) δ 33.13, 33.66, 126.69, 128.43, 128.72, 128.81, 131.11, 132.19, 132.30, 134.62, 136.15, 137.24, 148.25, 153.58 (br s), 168.24, 176.03 (br s); HRMS (ESI) m/z calculated for $\text{C}_{18}\text{H}_{16}\text{N}_4\text{O}_2\text{S}_2\text{Cl}$ $[\text{M}+\text{H}]^+$ 419.0403, found 419.0414; HPLC purity, 88.30%, $t_R = 10.63$ min.

6-((4-Chlorobenzyl)thio)-4-((2,6-difluorobenzyl)thio)-1,3,5-triazin-2(1H)-one (**35**). The compound was purified by crystallization from CH_3CN (5 mL). Yield, 64% (71 mg); white crystals; $R_f = 0.40$ ($\text{CH}_2\text{Cl}_2/\text{MeOH} = 15/1$); ^1H NMR (400 MHz, $\text{DMSO}-d_6$) δ 4.37 (s, 2H, SCH_2), 4.43 (s, 2H, SCH_2), 7.10–7.18 (m, 2H, Ar-H), 7.36–7.40 (m, 2H, Ar-H), 7.41–7.48 (m, 3H, Ar-H), 13.09 (br s, 1H, NHCO); ^{13}C NMR (100 MHz, $\text{DMSO}-d_6$) δ 21.39, 32.73, 111.76 (d, $^2J_{\text{FC}} = 24.9$ Hz), 111.88 (dd, $^2J_{\text{FC}} = 19.0$ Hz, $^2J_{\text{FC}} = 15.4$ Hz), 128.42, 130.44 (dd, $^3J_{\text{FC}} = 10.3$ Hz, $^3J_{\text{FC}} = 10.3$ Hz), 130.86, 131.98, 135.97, 149.90, 153.24 (br s), 160.60 (dd, $^1J_{\text{FC}} = 248.7$ Hz, $^3J_{\text{FC}} = 7.3$ Hz), 173.13 (br s); HRMS (ESI) m/z calculated for $\text{C}_{17}\text{H}_{13}\text{N}_3\text{O}_2\text{S}_2\text{ClF}_2$ $[\text{M}+\text{H}]^+$ 412.0157, found 412.0162; HPLC purity, 99.44%, $t_R = 17.06$ min.

3-(((6-((4-Chlorobenzyl)thio)-4-oxo-4,5-dihydro-1,3,5-triazin-2-yl)thio)methyl)benzoic acid (**36**). The compound was purified by crystallization from CH_3CN (5 mL). Yield, 59% (61 mg); white crystals; $R_f = 0.24$ ($\text{CH}_2\text{Cl}_2/\text{MeOH}/\text{CH}_3\text{COOH} = 15/1/0.1$); ^1H NMR (400 MHz, $\text{DMSO}-d_6$) δ (s, 2H, SCH_2), 4.43 (s, 2H, SCH_2), 7.35–7.47 (m, 5H, Ar-H), 7.64 (dt, $J_1 = 7.8$ Hz, $J_2 = 1.0$ Hz, 1H, Ar-H), 7.83 (dt, $J_1 = 7.8$ Hz, $J_2 = 1.3$ Hz, 1H, Ar-H), 7.97–8.00 (m, 1H, Ar-H), 13.03 (br s, 2H, COOH and NHCO); ^{13}C NMR (100 MHz, $\text{DMSO}-d_6$) δ 32.77, 33.09, 128.25, 128.41, 128.77, 129.76, 130.82, 130.94, 131.95, 133.42, 135.93, 137.51, 149.14, 153.06 (br s), 166.99, 176.12 (br s); HRMS (ESI) m/z calculated for $\text{C}_{18}\text{H}_{15}\text{N}_3\text{O}_3\text{S}_2\text{Cl}$ $[\text{M}+\text{H}]^+$ 420.0243, found 420.0242; HPLC purity, 99.46%, $t_R = 12.45$ min.

6-((4-Chlorobenzyl)thio)-4-((3-fluoro-5-(trifluoromethyl)benzyl)thio)-1,3,5-triazin-2(1H)-one (**37**). The compound was purified by trituration in *n*-hexanes and subsequent filtration. Yield, 71% (49 mg); white amorphous solid; $R_f = 0.28$ ($\text{CH}_2\text{Cl}_2/\text{MeOH} = 15/1$); ^1H NMR (400 MHz, $\text{DMSO}-d_6$) δ 4.34 (s, 2H, SCH_2), 4.44 (s, 2H, SCH_2), 7.34–7.42 (m, 4H, Ar-H), 7.55–7.62 (m, 2H, Ar-H), 7.66–7.69 (m, 1H, Ar-H), 13.07 (br s, 1H, NHCO); ^{13}C NMR (100 MHz, $\text{DMSO}-d_6$) δ 32.66, 32.90, 111.80 (dq, $^2J_{\text{FC}} = 24.9$ Hz, $^3J_{\text{FC}} = 3.7$ Hz), 120.26 (d, $^2J_{\text{FC}} = 22.0$ Hz), 122.14 (q, $^3J_{\text{FC}} = 4.4$ Hz), 123.35 (qd, $^1J_{\text{FC}} = 272.2$ Hz, $^4J_{\text{FC}} = 2.9$ Hz), 128.50, 130.92, 130.99 (qd, $^2J_{\text{FC}} = 33.7$ Hz, $^3J_{\text{FC}} = 6.6$ Hz), 132.13, 136.02, 142.22 (d, $^3J_{\text{FC}} = 8.1$ Hz), 150.07, 153.38 (br s), 160.63, 163.09, 175.80 (br s); 127.26, 127.62, 128.78, 130.32, 132.85, 139.48, 148.81, 153.04 (br s), 161.75 (d, $^1J_{\text{FC}} = 247.2$ Hz), 172.74 (br s); HRMS (ESI) m/z calculated for $\text{C}_{18}\text{H}_{13}\text{N}_3\text{O}_2\text{S}_2\text{ClF}_4$ $[\text{M}+\text{H}]^+$ 462.0125, found 462.0138; HPLC purity, 97.67%, $t_R = 19.08$ min.

6-((4-Chlorobenzyl)thio)-4-((2,4,5-trifluorobenzyl)thio)-1,3,5-triazin-2(1H)-one (**38**). The compound was purified by crystallization from CH_3CN (5 mL). Yield, 53% (32 mg); white crystals; $R_f = 0.37$ ($\text{CH}_2\text{Cl}_2/\text{MeOH} = 15/1$); ^1H NMR (400 MHz, $\text{DMSO}-d_6$) δ 4.33 (s, 2H, SCH_2), 4.35 (s, 2H, SCH_2), 7.35–7.39 (m, 2H, Ar-H), 7.40–7.44 (m, 2H, Ar-H), 7.52–7.64 (m, 2H, Ar-H), 13.08 (br s, 1H, NHCO); ^{13}C NMR (100 MHz, $\text{DMSO}-d_6$) δ 26.65, 32.71, 106.00 (dd, $^2J_{\text{FC}} = 27.1$ Hz, $^2J_{\text{FC}} = 21.3$ Hz), 119.08 (dd, $^2J_{\text{FC}} = 19.8$ Hz, $^3J_{\text{FC}} = 5.1$ Hz), 120.97 (dd, $^2J_{\text{FC}} = 19.1$ Hz, $^3J_{\text{FC}} = 4.9$ Hz), 128.40, 130.82, 131.98, 135.93, 145.53 (ddd, $^1J_{\text{FC}} = 241.4$ Hz, $^2J_{\text{FC}} = 13.2$ Hz, $^4J_{\text{FC}} = 4.4$ Hz), 148.65 (ddd, $^1J_{\text{FC}} = 248.0$ Hz, $^2J_{\text{FC}} = 16.2$ Hz, $^3J_{\text{FC}} = 13.2$ Hz), 149.90, 153.08 (br s), 155.60 (ddd, $^1J_{\text{FC}} = 245.0$ Hz, $^3J_{\text{FC}} = 9.5$ Hz, $^4J_{\text{FC}} = 2.2$ Hz), 175.14 (br s); HRMS (ESI) m/z calculated for $\text{C}_{17}\text{H}_{12}\text{N}_3\text{O}_2\text{S}_2\text{ClF}_3$ $[\text{M}+\text{H}]^+$ 430.0062, found 430.0062; HPLC

purity, 97.63%, $t_R = 17.70$ min.

2-((4-(((6-((4-Chlorobenzyl)thio)-4-oxo-4,5-dihydro-1,3,5-triazin-2-yl)thio)methyl)phenyl)propanoic acid (**39**). The compound was purified by crystallization from CH_3CN (5 mL). Yield, 46% (20 mg); white crystals; $R_f = 0.22$ ($\text{CH}_2\text{Cl}_2/\text{MeOH}/\text{CH}_3\text{COOH} = 15/1/0.1$); ^1H NMR (400 MHz, $\text{DMSO}-d_6$) δ 1.33 (d, $J = 7.1$ Hz, 3H, Ar-(CH) CH_3), 3.65 (q, $J = 7.1$ Hz, 1H, Ar-(CH) CH_3), 4.33 (s, 2H, SCH_2), 4.36 (s, 2H, SCH_2), 7.20–7.25 (m, 2H, Ar-H), 7.31–7.40 (m, 4H, Ar-H), 7.41–7.45 (m, 2H, Ar-H), 12.34 (br s, 1H, COOH), 13.00 (br s, 1H, NHCO); ^{13}C NMR (100 MHz, $\text{DMSO}-d_6$) δ 18.42, 32.78, 33.26, 44.29, 127.59, 128.44, 129.11, 130.85, 131.96, 135.07, 136.07, 140.44, 149.91, 153.34 (br s), 173.72 (br s), 175.26; HRMS (ESI) m/z calculated for $\text{C}_{20}\text{H}_{19}\text{N}_3\text{O}_3\text{S}_2\text{Cl}$ $[\text{M}+\text{H}]^+$ 448.0556, found 448.0550; HPLC purity, 98.27%, $t_R = 13.63$ min.

6-((4-Chlorobenzyl)thio)-4-((4-(hydroxymethyl)benzyl)thio)-1,3,5-triazin-2(1H)-one (**40**). The compound was purified by trituration in *n*-hexanes and subsequent filtration. Yield, 61% (43 mg); white amorphous solid; $R_f = 0.23$ ($\text{CH}_2\text{Cl}_2/\text{MeOH} = 15/1$); ^1H NMR (400 MHz, $\text{DMSO}-d_6$) δ 4.34 (s, 2H, SCH_2), 4.36 (s, 2H, SCH_2), 4.46 (s, 2H, Ar- CH_2OH), 7.23–7.28 (m, 2H, Ar-H), 7.31–7.35 (m, 2H, Ar-H), 7.35–7.40 (m, 2H, Ar-H), 7.40–7.45 (m, 2H, Ar-H), resonances for OH and NHCO missing; ^{13}C NMR (100 MHz, $\text{DMSO}-d_6$) δ 32.91, 33.57, 62.65, 126.72, 128.53, 128.87, 130.92, 132.07, 134.81, 136.11, 141.85, 150.02, 156.50 (br s), 172.13 (br s); HRMS (ESI) m/z calculated for $\text{C}_{18}\text{H}_{17}\text{N}_3\text{O}_2\text{S}_2\text{Cl}$ $[\text{M}+\text{H}]^+$ 406.0451, found 406.0454; HPLC purity, 97.33%, $t_R = 12.03$ min.

6-((4-Chlorobenzyl)thio)-4-((3-hydroxybenzyl)thio)-1,3,5-triazin-2(1H)-one (**41**). The compound was purified by trituration in *n*-hexanes and subsequent filtration. Yield, 64% (37 mg); white amorphous solid; $R_f = 0.45$ ($\text{CH}_2\text{Cl}_2/\text{MeOH} = 15/1$); ^1H NMR (400 MHz, $\text{DMSO}-d_6$) δ 4.28 (s, 2H, SCH_2), 4.36 (s, 2H, SCH_2), 6.66 (ddd, $J_1 = 8.0$ Hz, $J_2 = 2.4$ Hz, $J_3 = 0.9$ Hz, 1H, Ar-H), 6.76–6.81 (m, 2H, Ar-H), 7.07–7.13 (m, 1H, Ar-H), 7.35–7.45 (m, 4H, Ar-H), 9.46 (br s, 1H, Ar-OH), resonance for NHCO missing; ^{13}C NMR (100 MHz, $\text{DMSO}-d_6$) δ 32.85, 33.64, 114.50, 115.72, 119.58, 128.47, 129.58, 130.86, 132.01, 136.06, 137.73, 149.95, 153.18 (br s), 157.44, 173.88 (br s); HRMS (ESI) m/z calculated for $\text{C}_{17}\text{H}_{15}\text{N}_3\text{O}_2\text{S}_2\text{Cl}$ $[\text{M}+\text{H}]^+$ 392.0294, found 392.0302; HPLC purity, 96.77%, $t_R = 13.28$ min.

6-((4-Chlorobenzyl)thio)-4-((4-(trifluoromethyl)benzyl)thio)-1,3,5-triazin-2(1H)-one (**42**). The compound was purified by trituration in *n*-hexanes and subsequent filtration. Yield, 54% (34 mg); white amorphous solid; $R_f = 0.45$ ($\text{CH}_2\text{Cl}_2/\text{MeOH} = 15/1$); ^1H NMR (400 MHz, $\text{DMSO}-d_6$) δ 4.35 (s, 2H, SCH_2), 4.44 (s, 2H, SCH_2), 7.34–7.38 (m, 2H, Ar-H), 7.38–7.43 (m, 2H, Ar-H), 7.59–7.63 (m, 2H, Ar-H), 7.66–7.70 (m, 2H, Ar-H), resonances for OH and NHCO missing; ^{13}C NMR (100 MHz, $\text{DMSO}-d_6$) δ 32.81, 32.97, 124.10 (q, $^1J_{\text{FC}} = 271.4$ Hz), 125.35 (q, $^3J_{\text{FC}} = 6.8$ Hz), 128.48, 129.30 (q, $^2J_{\text{FC}} = 27.9$ Hz), 129.78, 130.87, 132.05, 135.97, 142.08, 148.10, 151.26 (br s), 171.87 (br s); HRMS (ESI) m/z calculated for $\text{C}_{18}\text{H}_{14}\text{N}_3\text{O}_2\text{S}_2\text{ClF}_3$ $[\text{M}+\text{H}]^+$ 444.0219, found 444.0217; HPLC purity, 95.03%, $t_R = 18.80$ min.

4.3. Molecular docking calculations

The molecular docking experiments were performed using GOLD docking tool [36] and the human topo II α ATPase domain (PDB: 1ZXN) [60]. In the first step, the validation of GOLD docking tool was performed [61] in the same way as in our previous studies [30–32] by redocking the native ligand AMP-PNP molecule into its binding site. To summarize, the active site was defined as 10 Å radius around the reference ligand AMP-PNP and hydrogen atoms were added to the protein. Magnesium ion and all waters were removed except for W924 and W931. They were included in docking calculations because it was previously assumed that they play an important role in the binding of the AMP-PNP molecule

[34]. AMP-PNP molecule was docked into the defined active site by applying the following parameters of the GOLD genetic algorithm (GA): Population size = 100, Selection pressure = 1.1, No. of Operations = 100000, No of Islands = 5, Niche size = 2, Migrate = 10, Mutate = 95, Crossover = 95. Different spin states of the water molecules W924 and W931 were allowed during the docking procedure. As in previous studies to insure that interactions similar to the interaction pattern of the purine moiety in the AMP-PNP molecule would be obtained, a pharmacophore constrain to Asn120 was added [60] and GoldScore scoring function was used. Obtained binding pose of the docked AMP-PNP closely resembled the experimentally determined, with the best RMSD agreement of 0.9 Å what indicated that used docking settings are reliable (Fig. S1). The same scoring function and the described docking settings were used for the molecular docking calculations when virtual screening of the generated focused chemical library was performed. The 1,3,5-triazin-2(1H)-one core was modeled as a keto tautomer, the preferred tautomeric form according to the X-ray and quantum mechanical investigations [62].

4.4. Molecular dynamics simulation and dynophore calculations

Molecular Dynamics (MD) simulation using a monomer of the human topo II α ATPase domain (PDB: 1ZXN) with the docked conformation of the selective active compound **25** was performed using CHARMM molecular modeling suite [63]. The bound conformations in the ATP binding site were generated as described in previous section using GOLD molecular docking suite [36]. The crystal structure of protein was prepared and then simulated in a similar fashion as described previously [30–32,64]. CHARMM-GUI environment was utilized for the protein manipulation and construction of the solvated protein-compound complexes [65]. CHARMM parameter and topology files (version 36) were utilized to specify the force field parameters of the amino acid residues comprising the protein [66,67]. CHARMM General Force Field (CGenFF) was used to describe the atom types and partial charges of active compound **25** [68]. Determined partial charges and assigned atom types for this compound are listed in the Supplementary material (Table S1). The protein-ligand system was immersed into a sphere TIP3 of water molecules [69] with truncated octahedral shape with the edge distance of 10 Å and 3 chlorine ions were added to make the system electroneutral. Ion placement was performed using Monte Carlo method. The periodic boundary conditions (PBC) were applied based on the shape and size of the system. Grid information for the Particle-mesh Ewald (PME) Fast Fourier Transform (FFT) was generated automatically. The final system prepared for the MD simulation was comprised of 73266 atoms. Short energy minimizations were then performed to remove bad contacts. The system was then minimized for 10000 steps by steepest descent (SD) method followed by 10000 steps of modified Adopted Basis Newton–Raphson (ABNR) method and an MD equilibration run of 1 ns. Production MD trajectory was generated using leapfrog integration scheme and 2 fs simulation step using SHAKE algorithm. A 20 ns long MD simulation production run was performed. Conformations were sampled every 500th step resulting in 10,000 conformations for subsequent analysis. Visualization and analysis of the geometry parameters of the production MD trajectory was performed using VMD program [70]. RMSD of compound **25** was calculated against the initial docking conformation, taking heavy atoms into account. Further inspection of the overall conformational behavior for the MD simulation can also be seen in the generated two movie animations (see [Supporting information animations](#)).

To further provide a more comprehensive outlook of the observed dynamical interaction pattern between the simulated

ligand **25** and the ATP binding site, 1000 exported MD equidistant frames were used in the dynamic pharmacophore analysis using DynophoreApp [52,53,71] developed in the Molecular Design Lab of Prof. Wolber at Freie Universität Berlin. These calculations resulted in a dynophore model that was subsequently analyzed. These dynophore calculations were performed on computers of the Molecular Design Lab, Germany and subsequently visualized in LigandScout (see also Supplementary material for additional dynophore results) [37].

4.5. HTS relaxation assay of human topo II α

The HTS topo II α relaxation assay was performed on the black streptavidin-coated 96-well microtiter plate. Plate was rehydrated using wash buffer (20 mM Tris–HCl (pH = 7.6), 137 mM NaCl, 0.005% (w/v) BSA, 0.05% (v/v) TWEEN-20[®]) and biotinylated oligonucleotide was immobilized onto the wells. Next, the excess oligonucleotide was washed off with wash buffer. Enzyme assay was carried out in reaction volume of 30 μ L using 0.75 μ g supercoiled plasmid pNO1 as a substrate and human topo II α . Enzyme was diluted to the appropriate concentration with dilution buffer comprised of 50 mM Tris-HCl (pH = 7.5), 100 mM NaCl, 1 mM DTT, 0.5 mM EDTA, 50% (v/v) glycerol and 50 μ g/ml albumin. Tested compounds (0.3 μ L) were added as a stock solution in DMSO and final concentration of DMSO was 1%, respectively. Reactions were incubated at 37 °C for 30 min, and TF buffer (50 mM NaOAc (pH = 5.0), 50 mM NaCl, 50 mM MgCl₂) was added to the wells and incubated at room temperature for additional 30 min to allow the triplex biotin-oligonucleotide-plasmid formation [39]. To eliminate the aggregation and non-specific inhibition a surfactant (TWEEN-20[®]) was added to the reaction mixture [72]. Unbound plasmid was washed off with TF buffer and stained with the DNA-detection Dye in the T10 buffer (10 mM Tris–HCl (pH = 8) and 1 mM EDTA) was added. After mixing, fluorescence was read using Tecan fluorimeter (Excitation: 485 nm and Emission: 535 nm). Screening was performed at the inhibitor concentrations of 7.8, 31.5, 125 and 500 μ M. IC₅₀ values were calculated using GraphPad Prism 6.0 software [73] and represent the concentrations of inhibitors where residual activity of the enzyme was 50% [39].

4.6. The human topo II α and human topo II β decatenation assay

The human topo II decatenation assay kit from Inspiralis (Norwich, UK) was used to determine if compounds inhibit the DNA decatenation [74,75]. One U of human topo II (α or β) was incubated with 200 ng kDNA in a 30 μ L reaction at 37 °C for 30 min under the following conditions: 50 mM Tris HCl (pH 7.5), 125 mM NaCl, 10 mM MgCl₂, 5 mM DTT, 0.5 mM EDTA, 0.1 mg/ml bovine serum albumin (BSA) and 1 mM ATP. Compounds **13**, **18** and **25** were serially diluted in DMSO and added to the reaction mixture before the addition of the enzyme. Etoposide was used as a control compound. Each reaction was then stopped by the addition of 30 μ L chloroform/iso-amyl alcohol (26:1) and 30 μ L Stop Dye (40% sucrose (w/v), 100 mM Tris.HCl (pH 7.5), 10 mM EDTA, 0.5 μ g/ml bromophenol blue), before being loaded on a 1% TAE gel run at 85 V for 90 min. Assays were performed at 4 concentrations of ligand: 3.9, 31.5, 125 and 500 μ M. The final DMSO concentration in all reactions was 1% (v/v).

Bands were visualized by the ethidium bromide staining for 15 min and destaining for subsequent 10 min. Gels were scanned using the documentation equipment (GeneGenius, Syngene, Cambridge, UK) and inhibition levels were calculated from band data obtained with gel scanning software (GeneTools, Syngene, Cambridge, UK). Experiment was performed in duplicates for all compounds.

4.7. The human topo II α cleavage and competitive cleavage assay

The human topo II α cleavage assay was performed in collaboration with Inspiralis (Norwich, UK). One U of human topo II α was incubated with the 0.5 μ g supercoiled plasmid DNA (pBR322) and the respective amount of selected active compounds **13**, **18** and **25** or reference compound etoposide in a 30 μ l reaction at 37 °C for 60 min under the following conditions: 20 mM Tris HCl (pH 7.5), 200 mM NaCl, 0.25 mM EDTA and 5% glycerol. Selected compounds were tested at four concentrations: 3.9, 31.5, 125 and 500 μ M. The reaction was then incubated for additional 30 min with 0.2% SDS and 0.5 μ g/ μ l proteinase K. Subsequently the reaction was stopped by adding 30 μ l of chloroform/iso-amyl alcohol (26:1) and 30 μ l of Stop Dye (40% sucrose (w/v), 100 mM Tris.HCl (pH 7.5), 10 mM EDTA, 0.5 μ g/ml bromophenol blue), before sample being loaded on the 1% TAE gel run at 80 V for 2 h.

Bands were visualized by the ethidium bromide staining for 15 min and destaining for subsequent 10 min. Gels were scanned using the documentation equipment (GeneGenius, Syngene, Cambridge, UK) and cleavage levels were calculated from the band data obtained by the gel scanning software (GeneTools, Syngene, Cambridge, UK).

The competitive cleavage assay was performed as described above, with the difference that the fixed concentration of etoposide **1** (50 μ M) was added to the assayed compounds **13**, **18** and **25** at 3.9, 31.5, 125, 500 μ M concentrations. The necessary amount of etoposide required for optimal cleavage (i.e. the amount which causes maximum cleavage) was determined by prior titration. Total DMSO in the assay was 2% (cumulative effect of adding 2 different compounds). The DNA was tested in various control conditions (reaction with human topo II α only, without human topo II α , with human topo II α in 1% DMSO) to check for the background cleavage. Cleavage and competitive cleavage assays were performed in duplicates for all compounds.

4.8. Human topoisomerase II ATPase assays at different concentration of ATP – competitive ATPase assay

The human topo competitive ATPase assay was performed in collaboration with Inspiralis (Norwich, UK). Selected active compounds **18** and **25** were dissolved and diluted in DMSO and added to the reaction before the addition of the enzyme. Compounds were analyzed using a linked ATPase assay in which the ADP produced by the hydrolysis of ATP leads to the conversion of NADH to NAD by a pyruvate kinase/lactate dehydrogenase mix. The disappearance of NADH was monitored at 340 nm [42].

A mix of the assay buffer (5 μ l of 10X buffer per assay: final conc. 20 mM Tris-HCl, 5 mM magnesium acetate, 125 mM potassium acetate, 2 mM DTT, pH 7.9), linear pBR322 (1.5 μ l of 1 mg/ml per assay), phosphoenol pyruvate (0.5 μ l of 80 mM per assay), pyruvate kinase/lactate dehydrogenase mix (0.75 μ l per assay), NADH (1 μ l of 20 mM per assay), DMSO (1.5 μ l per assay), and water (32.85 μ l per assay) was made. 39.1 μ l of this mixture was aliquoted into the wells of a 384-well microtiter plate. 2.5 μ l of DMSO or the investigated compound were added to the wells and mixed. 5 μ l of the dilution buffer or human topo II α (120 nM stock giving the 12 nM final concentration) were then added and mixed. A pre-run was done before the run was started by adding 3.4 μ l of the appropriate concentration of ATP and the OD340 monitored for up to 30 min. Assays were performed at 37 °C. Two negative controls (5% DMSO and dilution buffer without enzyme) were run in the presence of 2 mM ATP. This assay was performed at 8 different concentrations of the ATP (0.025, 0.05, 0.075, 0.1, 0.25, 0.5, 0.75 and 1 mM). Assays were performed at 10, 25, 40, and 50 μ M final concentrations of the investigated compounds **18** and **25**. The final DMSO concentration

in all the reactions was 5% (v/v). Assay was performed in duplicates.

4.9. Cytotoxicity measurements in MCF-7 and HepG2 cell lines using MTS assay

In vitro cytotoxicity of investigated compounds was evaluated in two human cancer cell lines: the breast cancer MCF-7 and hepatocellular carcinoma HepG2 cell lines. The HepG2 cells (ATCC) were cultivated at 37 °C and 5% CO₂ in MEME medium (M2414, Sigma) supplemented with 10% FBS, 2 mM L-Glutamine, 1% NEAA, 2.2 g/L NaHCO₃, 1 mM sodium pyruvate and 100 IU/ml penicillin/streptomycin and MCF-7 (ATCC) were cultivated in Eagle's MEM medium (M5650, Sigma), supplemented with 10% fetal bovine serum, 2 mM glutamine, and 100 IU/ml penicillin/streptomycin. After the exposure to the tested compounds the viability of the MCF-7 and HepG2 cells was determined by MTS tetrazolium reduction assay.

The cells were seeded onto 96-well microplates (Nunc, Termo-Fisher Scientific, Waltham, MA, USA) at densities of 8000 cells per well (HepG2) and 7000 cells per well (MCF-7) in 200 μ l growth medium and incubated overnight to attach. The next day, the growth medium was replaced by the fresh complete growth medium containing appropriate concentrations of the compounds. Prepared microplates were then incubated for an additional 24 h and after 40 μ l of freshly prepared MTS: PMS solution (20:1) was added directly to the 200 μ l of medium in the culture wells and incubated for additional 3 h (37 °C, 5% CO₂). Finally, the absorbance was measured at wavelength of 490 nm using a Microplate Reader (Synergy MX, BioTek, Winooski, VT, USA). As positive control, etoposide at 200 μ M was used. Cell viability was determined by comparing the OD (optical density) of the wells containing the cells treated with investigated compounds with solvent control cells those of unexposed cells and presented as % of cell viability \pm SD. Experiments were performed in five replicates. EC₅₀ values were calculated by non-linear regression analysis using GraphPad Prism 7.0 Software. Statistical significance between treated groups and the control was determined by One-way analysis of variance and Dunnett's Multiple Comparison Test.

4.10. Analyses of the induction of DNA double strand breaks by γ -H2AX assay

The HepG2 cells were seeded on the 25 cm² plates (Corning Inc., NY, USA) (750 000 cells/plate), left to attach overnight and were subsequently exposed to the selected compound **25** (0.75 μ M and 40 μ M) and etoposide (positive control, 50 μ M) for 24 h. After the exposure the floating and adherent cells were collected by trypsinization. For the fixation, the cells were centrifuged at 1000 rpm, 4 °C for 5 min, washed twice with ice cold PBS, resuspended in 0.5 mL cold PBS and ethanol (1.5 mL) was added drop wise into the cell pellet, while vortexing. The cells were fixed at 4 °C overnight and stored at –20 °C until analysis. Fixed cells were centrifuged at 1200 rpm for 10 min, washed with ice cold 1 \times PBS and labelled with Anti-H2AX pS139 antibodies according to manufacturer's protocol (Miltenyi Biotec, Germany). Flow cytometric analysis was carried out on a MACSQuant Analyzer 10 (Miltenyi Biotec, Germany). APC intensity, corresponding to DSBs, was detected in the APC-A channel. Unspecific binding was checked with reagent APC antibodies (Miltenyi Biotec, Germany). In each sample, 10 000 events were recorded. Independent experiments were repeated three times. In all experiments, 50 μ M etoposide was included as positive control and 0.5% DMSO as solvent control. For further analysis the raw data (APC intensities of each cell obtained as APC-A values) was exported from MACSQuantify software and it was converted to .fcs format and further to the .csv format. Statistical analysis was performed with R statistic program, free available on the web.

Acknowledgement

This work was supported by the Ministry of Education, Science and Sport of the Republic of Slovenia through the Research program grants P1-0012, P1-0245 and P-0208 as well as a Young Researcher Grant to K.B. M. J. was supported by the International Program Associate program at RIKEN Yokohama. Dr. Nicolas Burton and Dr. Alison Howells from Inspiralis, Norwich, UK are acknowledged for performing human DNA topoisomerase II α decatenation, cleavage and ATPase assays. Maruša Klemenčič, M. Pharm is acknowledged for synthesizing several compounds discussed in this work. Prof. Gerhard Wolber is acknowledged and thanked for providing us access to the dynophore calculations at the computer cluster of the Freie Universität Berlin, Germany. Klara Hercog from the National institute of Biology in Ljubljana is acknowledged for her help with the data analysis of the results obtained in the γ -H2AX assay.

Appendix A. Supplementary data

Supplementary data to this article can be found online at <https://doi.org/10.1016/j.ejmech.2019.04.055>.

References

- [1] National Cancer Institute. www.cancer.gov (accessed 25.10.2018).
- [2] Cancer, Nature, 509 S49–S96.
- [3] D. Hanahan, R.A. Weinberg, The hallmarks of cancer, Cell 100 (2000) 57–70.
- [4] D. Hanahan, R.A. Weinberg, Hallmarks of cancer: the next generation, Cell 144 (2011) 646–674.
- [5] J.L. Nittiss, DNA topoisomerase II and its growing repertoire of biological functions, Nat. Rev. Canc. 9 (2009) 327–337.
- [6] Y. Pommier, DNA topoisomerase I inhibitors: chemistry, biology, and interfacial inhibition, Chem. Rev. 109 (2009) 2894–2902.
- [7] J.M. Berger, S.J. Gamblin, S.C. Harrison, J.C. Wang, Structure and mechanism of DNA topoisomerase II, Nature 379 (1996) 225–232.
- [8] J.J. Champoux, DNA topoisomerases: structure, function, and mechanism, Annu. Rev. Biochem. 70 (2001) 369–413.
- [9] A.J. Schoeffler, J.M. Berger, DNA topoisomerases: harnessing and constraining energy to govern chromosome topology, Q. Rev. Biophys. 41 (2008) 41–101.
- [10] A. Sharma, A. Mondragon, DNA topoisomerases, Curr. Opin. Struct. Biol. 5 (1995) 39–47.
- [11] J.C. Wang, DNA topoisomerases: why so many? J. Biol. Chem. 266 (1991) 6659–6662.
- [12] S.M. Vos, E.M. Tretter, B.H. Schmidt, J.M. Berger, All tangled up: how cells direct, manage and exploit topoisomerase function, Nat. Rev. Mol. Cell Biol. 12 (2011) 827–841.
- [13] A. Vologodskii, Energy transformation in biological molecular motors, Phys. Life Rev. 3 (2006) 119–132.
- [14] A. Vologodskii, Disentangling DNA molecules, Phys. Life Rev. 18 (2016) 118–134.
- [15] T.T. Harkins, J.E. Lindsley, Pre-steady-state analysis of ATP hydrolysis by *Saccharomyces cerevisiae* DNA topoisomerase II. 1. A DNA-dependent burst in ATP hydrolysis, Biochemistry 37 (1998) 7292–7298.
- [16] J.E. Deweese, N. Osheroff, The DNA cleavage reaction of topoisomerase II: wolf in sheep's clothing, Nucleic Acids Res. 37 (2009) 738–748.
- [17] F.H. Drake, J.P. Zimmerman, F.L. McCabe, H.F. Bartus, S.R. Per, D.M. Sullivan, W.E. Ross, M.R. Mattern, R.K. Johnson, S.T. Crooke, et al., Purification of topoisomerase II from amsacrine-resistant P388 leukemia cells. Evidence for two forms of the enzyme, J. Biol. Chem. 262 (1987) 16739–16747.
- [18] G. Capranico, S. Tinelli, C.A. Austin, M.L. Fisher, F. Zunino, Different patterns of gene expression of topoisomerase II isoforms in differentiated tissues during murine development, Biochim. Biophys. Acta 1132 (1992) 43–48.
- [19] M. Watanabe, K. Tsutsui, K. Tsutsui, Y. Inoue, Differential expressions of the topoisomerase II alpha and II beta mRNAs in developing rat brain, Neurosci. Res. 19 (1994) 51–57.
- [20] K. Tsutsui, K. Tsutsui, O. Hosoya, K. Sano, A. Tokunaga, Immunohistochemical analyses of DNA topoisomerase II isoforms in developing rat cerebellum, J. Comp. Neurol. 431 (2001) 228–239.
- [21] J.L. Delgado, C.M. Hsieh, N.L. Chan, H. Hiasa, Topoisomerases as anticancer targets, Biochem. J. 475 (2018) 373–398.
- [22] B. Pogorelnik, A. Perdih, T. Solmajer, Recent developments of DNA poisons - human DNA topoisomerase II alpha inhibitors - as anticancer agents, Curr. Pharmaceut. Des. 19 (2013) 2474–2488.
- [23] W. Hu, X.S. Huang, J.F. Wu, L. Yang, Y.T. Zheng, Y.M. Shen, Z.Y. Li, X. Li, Discovery of novel topoisomerase II inhibitors by medicinal chemistry approaches, J. Med. Chem. 61 (2018) 8947–8980.
- [24] C. Bailly, Contemporary challenges in the design of topoisomerase II inhibitors for cancer chemotherapy, Chem. Rev. 112 (2012) 3611–3640.
- [25] G. Minotti, P. Menna, E. Salvatorelli, G. Cairo, L. Gianni, Anthracyclines: molecular advances and pharmacologic developments in antitumor activity and cardiotoxicity, Pharmacol. Rev. 56 (2004) 185–229.
- [26] C.A. Felix, Secondary leukemias induced by topoisomerase-targeted drugs, Biochim. Biophys. Acta 1400 (1998) 233–255.
- [27] E.L. Baldwin, N. Osheroff, Etoposide, topoisomerase II and cancer, Curr. Med. Chem. Anti Cancer Agents 5 (2005) 363–372.
- [28] E.M. Nelson, K.M. Tewey, L.F. Liu, Mechanism of antitumor drug-action - poisoning of mammalian DNA topoisomerase-II on DNA by 4'-(9-acridinylamino)-methanesulfonate-meta-anisidide, Proc. Natl. Acad. Sci. U.S.A.-Biol. Sci. 81 (1984) 1361–1365.
- [29] B. Pogorelnik, A. Perdih, T. Solmajer, Recent advances in the development of catalytic inhibitors of human DNA topoisomerase II alpha as novel anticancer agents, Curr. Med. Chem. 20 (2013) 694–709.
- [30] B. Pogorelnik, M. Janežič, I. Sosić, S. Gobec, T. Solmajer, A. Perdih, 4,6-Substituted-1,3,5-triazin-2(1H)-ones as monocyclic catalytic inhibitors of human DNA topoisomerase IIalpha targeting the ATP binding site, Bioorg. Med. Chem. 23 (2015) 4218–4229.
- [31] B. Pogorelnik, M. Brvar, I. Zajc, M. Filipič, T. Solmajer, A. Perdih, Monocyclic 4-amino-6-(phenylamino)-1,3,5-triazines as inhibitors of human DNA topoisomerase II α , Bioorg. Med. Chem. Lett. 24 (2014) 5762–5768.
- [32] B. Pogorelnik, M. Brvar, B. Zegura, M. Filipič, T. Solmajer, A. Perdih, Discovery of mono- and disubstituted 1H-Pyrazolo[3,4]pyrimidines and 9H-purines as catalytic inhibitors of human DNA topoisomerase II alpha, ChemMedChem 10 (2015) 345–359.
- [33] M. Janežič, B. Pogorelnik, M. Brvar, T. Solmajer, A. Perdih, 3-substituted-1 H-indazoles as Catalytic Inhibitors of the Human DNA Topoisomerase II α , ChemistrySelect 2 (2017) 480–488.
- [34] P. Furet, J. Schoepfer, T. Radimerski, P. Chene, Discovery of a new class of catalytic topoisomerase II inhibitors targeting the ATP-binding site by structure based design. Part I, Bioorg. Med. Chem. Lett. 19 (2009) 4014–4017.
- [35] I. Sosić, B. Mirković, S. Turk, B. Stefane, J. Kos, S. Gobec, Discovery and kinetic evaluation of 6-substituted 4-benzylthio-1,3, 5-triazin-2(1H)-ones as inhibitors of cathepsin B, Eur. J. Med. Chem. 46 (2011) 4648–4656.
- [36] G. Jones, P. Willett, R.C. Glen, A.R. Leach, R. Taylor, Development and validation of a genetic algorithm for flexible docking, J. Mol. Biol. 267 (1997) 727–748.
- [37] G. Wolber, T. Langer, LigandScout: 3-D pharmacophores derived from protein-bound ligands and their use as virtual screening filters, J. Chem. Inf. Model. 45 (2005) 160–169.
- [38] I. Sosić, B. Mirković, B. Stefane, A. Kovac, J. Kos, S. Gobec, Diversely substituted 1,3,5-triazines as hits in different drug discovery programs, Eur. J. Pharm. Sci. 44 (2011) 184–185.
- [39] A. Maxwell, N.P. Burton, N. O'Hagan, High-throughput assays for DNA gyrase and other topoisomerases, Nucleic Acids Res. 34 (2006).
- [40] W.B. Wu, J.B. Ou, Z.H. Huang, S.B. Chen, T.M. Ou, J.H. Tan, D. Li, L.L. Shen, S.L. Huang, L.Q. Gu, Z.S. Huang, Synthesis and evaluation of mansonone F derivatives as topoisomerase inhibitors, Eur. J. Med. Chem. 46 (2011) 3339–3347.
- [41] P. Chene, J. Rudloff, J. Schoepfer, P. Furet, P. Meier, Z. Qian, J.M. Schlaeppli, R. Schmitz, T. Radimerski, Catalytic inhibition of topoisomerase II by a novel rationally designed ATP-competitive purine analogue, BMC Chem. Biol. 9 (2009) 1.
- [42] K. Bergant, M. Janežič, A. Perdih, Bioassays and in silico methods in the identification of human DNA topoisomerase IIalpha inhibitors, Curr. Med. Chem. 25 (2018) 3286–3318.
- [43] D. Perrin, B. van Hille, B.T. Hill, Differential sensitivities of recombinant human topoisomerase IIalpha and beta to various classes of topoisomerase II-interacting agents, Biochem. Pharmacol. 56 (1998) 503–507.
- [44] E. Willmore, A.J. Frank, K. Padgett, M.J. Tilby, C.A. Austin, Etoposide targets topoisomerase IIalpha and IIbeta in leukemic cells: isoform-specific cleavable complexes visualized and quantified in situ by a novel immunofluorescence technique, Mol. Pharmacol. 54 (1998) 78–85.
- [45] E. Toyoda, S. Kagaya, I.G. Cowell, A. Kurosawa, K. Kamoshita, K. Nishikawa, S. Iizumi, H. Koyama, C.A. Austin, N. Adachi, NK314, a topoisomerase II inhibitor that specifically targets the alpha isoform, J. Biol. Chem. 283 (2008) 23711–23720.
- [46] N. Akimitsu, N. Adachi, H. Hirai, M.S. Hossain, H. Hamamoto, M. Kobayashi, Y. Aratani, H. Koyama, K. Sekimizu, Enforced cytokinesis without complete nuclear division in embryonic cells depleting the activity of DNA topoisomerase IIalpha, Genes Cells 8 (2003) 393–402.
- [47] X. Yang, W. Li, E.D. Prescott, S.J. Burden, J.C. Wang, DNA topoisomerase IIbeta and neural development, Science 287 (2000) 131–134.
- [48] A. Sakaguchi, A. Kikuchi, Functional compatibility between isoform alpha and beta of type II DNA topoisomerase, J. Cell Sci. 117 (2004) 1047–1054.
- [49] S. Kenig, V. Faoro, E. Bourkoulas, N. Podergajs, T. Ius, M. Vindigni, M. Skrap, T. Lah, D. Cesselli, P. Storici, A. Vindigni, Topoisomerase IIbeta mediates the resistance of glioblastoma stem cells to replication stress-inducing drugs, Cancer Cell Int. 16 (2016) 58.
- [50] P. Sledz, A. Caffisch, Protein structure-based drug design: from docking to molecular dynamics, Curr. Opin. Struct. Biol. 48 (2018) 93–102.
- [51] D. Sydow, Dynophores: novel dynamic pharmacophores, in: Humboldt-Universität zu Berlin, Lebenswissenschaftliche Fakultät, 2015.
- [52] A. Bock, M. Bermudez, F. Krebs, C. Matera, B. Chirinda, D. Sydow, C. Dallanocce,

- U. Holzgrabe, M. De Amici, M.J. Lohse, G. Wolber, K. Mohr, Ligand binding ensembles determine graded agonist efficacies at a G protein-coupled receptor, *J. Biol. Chem.* 291 (2016) 16375–16389.
- [53] B.S. Xie, H.C. Zhao, S.K. Yao, D.X. Zhuo, B. Jin, D.C. Lv, C.L. Wu, D.L. Ma, C. Gao, M. Bermudez, C. Rakers, G. Wolber, Structural characteristics of the allosteric binding site represent a key to subtype selective modulators of muscarinic acetylcholine receptors, *Mol Inform* 34 (2015) 526–530.
- [54] B.S. Xie, H.C. Zhao, S.K. Yao, D.X. Zhuo, B. Jin, D.C. Lv, C.L. Wu, D.L. Ma, C. Gao, X.M. Shu, Z.L. Ai, Autophagy inhibition enhances etoposide-induced cell death in human hepatoma G2 cells, *Int. J. Mol. Med.* 27 (2011) 599–606.
- [55] G. Gajski, M. Geric, B. Zegura, M. Novak, J. Nunic, D. Bajrektarevic, V. Garaj-Vrhovac, M. Filipic, Genotoxic potential of selected cytostatic drugs in human and zebrafish cells, *Environ. Sci. Pollut. Res. Int.* 23 (2016) 14739–14750.
- [56] G.K. Dasika, S.C. Lin, S. Zhao, P. Sung, A. Tomkinson, E.Y. Lee, DNA damage-induced cell cycle checkpoints and DNA strand break repair in development and tumorigenesis, *Oncogene* 18 (1999) 7883–7899.
- [57] D.J. Smart, H.D. Halicka, G. Schmuck, F. Traganos, Z. Darzynkiewicz, G.M. Williams, Assessment of DNA double-strand breaks and gammaH2AX induced by the topoisomerase II poisons etoposide and mitoxantrone, *Mutat. Res.* 641 (2008) 43–47.
- [58] O.A. Sedelnikova, E.P. Rogakou, I.G. Panyutin, W.M. Bonner, Quantitative detection of (125)IdU-induced DNA double-strand breaks with gamma-H2AX antibody, *Radiat. Res.* 158 (2002) 486–492.
- [59] E.P. Rogakou, C. Boon, C. Redon, W.M. Bonner, Megabase chromatin domains involved in DNA double-strand breaks in vivo, *J. Cell Biol.* 146 (1999) 905–916.
- [60] H. Wei, A.J. Ruthenburg, S.K. Bechis, G.L. Verdine, Nucleotide-dependent domain movement in the ATPase domain of a human type IIA DNA topoisomerase, *J. Biol. Chem.* 280 (2005) 37041–37047.
- [61] J. Kirchmair, P. Markt, S. Distinto, G. Wolber, T. Langer, Evaluation of the performance of 3D virtual screening protocols: RMSD comparisons, enrichment assessments, and decoy selection - what can we learn from earlier mistakes? *J. Comput. Aided Mol. Des.* 22 (2008) 213–228.
- [62] K. Srinivas, S. Sitha, B. Sridhar, V. Jayathirtha Rao, K. Bhanuprakash, K. Ravikumar, Tautomerism of bis(2,4-benzoyloxy)-6-(5H)-one-1,3,5-triazine: a combined crystallographic and quantum-chemical investigation, *Struct. Chem.* 17 (2006) 561–568.
- [63] B.R. Brooks, R.E. Bruccoleri, B.D. Olafson, D.J. States, S. Swaminathan, M. Karplus, Charmm - a program for macromolecular energy, minimization, and dynamics calculations, *J. Comput. Chem.* 4 (1983) 187–217.
- [64] B.R. Brooks, C.L. Brooks III, A.D. MacKerell Jr., L. Nilsson, R.J. Petrella, B. Roux, Y. Won, G. Archontis, C. Bartels, S. Boresch, A. Caffisch, L. Caves, Q. Cui, A.R. Dinner, M. Feig, S. Fischer, J. Gao, M. Hodoscek, W. Im, K. Kuczera, T. Lazaridis, J. Ma, V. Ovchinnikov, E. Paci, R.W. Pastor, C.B. Post, J.Z. Pu, M. Schaefer, B. Tidor, R.M. Venable, H.L. Woodcock, X. Wu, W. Yang, D.M. York, M. Karplus, CHARMM: the biomolecular simulation program, *J. Comput. Chem.* 30 (2009) 1545–1614.
- [65] S. Jo, T. Kim, V.G. Iyer, W. Im, Software news and updates - CHARNIM-GUI: a web-based graphical user interface for CHARMM, *J. Comput. Chem.* 29 (2008) 1859–1865.
- [66] A.D. MacKerell, D. Bashford, M. Bellott, R.L. Dunbrack, J.D. Evanseck, M.J. Field, S. Fischer, J. Gao, H. Guo, S. Ha, D. Joseph-McCarthy, L. Kuchnir, K. Kuczera, F.T.K. Lau, C. Mattos, S. Michnick, T. Ngo, D.T. Nguyen, B. Prodhom, W.E. Reiher, B. Roux, M. Schlenkrich, J.C. Smith, R. Stote, J. Straub, M. Watanabe, J. Wiorkiewicz-Kuczera, D. Yin, M. Karplus, All-atom empirical potential for molecular modeling and dynamics studies of proteins, *J. Phys. Chem. B* 102 (1998) 3586–3616.
- [67] A.D. MacKerell, M. Feig, C.L. Brooks, Extending the treatment of backbone energetics in protein force fields: limitations of gas-phase quantum mechanics in reproducing protein conformational distributions in molecular dynamics simulations, *J. Comput. Chem.* 25 (2004) 1400–1415.
- [68] K. Vanommeslaeghe, E. Hatcher, C. Acharya, S. Kundu, S. Zhong, J. Shim, E. Darian, O. Guvench, P. Lopes, I. Vorobyov, A.D. MacKerell, CHARMM general force field: a force field for drug-like molecules compatible with the CHARMM all-atom additive biological force fields, *J. Comput. Chem.* 31 (2010) 671–690.
- [69] W.L. Jorgensen, J. Chandrasekhar, J.D. Madura, R.W. Impey, M.L. Klein, Comparison of simple potential functions for simulating liquid water, *J. Chem. Phys.* 79 (1983) 926–935.
- [70] W. Humphrey, A. Dalke, K. Schulten, VMD: visual molecular dynamics, *J. Mol. Graph. Model.* 14 (1996) 33–38.
- [71] B. Nizami, D. Sydow, G. Wolber, B. Honarparvar, Molecular insight on the binding of NNRTI to K103N mutated HIV-1 RT: molecular dynamics simulations and dynamic pharmacophore analysis, *Mol. Biosyst.* 11 (2016) 3385–3395.
- [72] A.J. Ryan, N.M. Gray, P.N. Lowe, C.W. Chung, Effect of detergent on "promiscuous" inhibitors, *J. Med. Chem.* 46 (2003) 3448–3451.
- [73] L.J.C.U. GraphPad software, in.
- [74] T.R. Hammonds, A. Maxwell, The DNA dependence of the ATPase activity of human DNA topoisomerase IIalpha, *J. Biol. Chem.* 272 (1997) 32696–32703.
- [75] Osheroff Neil, B. Mary-Ann, DNA Topoisomerase Protocols 2000.